Title

CD47 masks pro-phagocytic ligands in cis on tumor cells to suppress antitumor immunity

Journal

Nature Immunology, 24(12)

ISSN

1529-2908

Authors

Tang, Zhenghai

Zhong, Ming-Chao

Qian, Jin

et al.

Publication Date

2023-12-01

DOI

10.1038/s41590-023-01671-2

Peer reviewed

nature immunology

Article

https://doi.org/10.1038/s41590-023-01671-2

CD47 masks pro-phagocytic ligands in *cis* on tumor cells to suppress antitumor immunity

Received: 15 February 2023

Accepted: 5 October 2023

Published online: 9 November 2023

Check for updates

Zhenghai Tang[1], Ming-Chao Zhong[1], Jin Qian[1], Cristian Camilo Galindo[1,2], Dominique Davidson[1], Jiaxin Li[1,2], Yunlong Zhao[3], Enfu Hui[3] & André Veillette[1,2,4]

Cancer cells often overexpress CD47, which triggers the inhibitory receptor SIRPα expressed on macrophages, to elude phagocytosis and antitumor immunity. Pharmacological blockade of CD47 or SIRPα is showing promise as anticancer therapy, although CD47 blockade has been associated with hematological toxicities that may reflect its broad expression pattern on normal cells. Here we found that, in addition to triggering SIRPα, CD47 suppressed phagocytosis by a SIRPα-independent mechanism. This mechanism prevented phagocytosis initiated by the pro-phagocytic ligand, SLAMF7, on tumor cells, due to a *cis* interaction between CD47 and SLAMF7. The CD47–SLAMF7 interaction was disrupted by CD47 blockade and by a first-in-class agonist SLAMF7 antibody, but not by SIRPα blockade, thereby promoting antitumor immunity. Hence, CD47 suppresses phagocytosis not only by engaging SIRPα, but also by masking cell-intrinsic pro-phagocytic ligands on tumor cells and knowledge of this mechanism may influence the decision between CD47 blockade or SIRPα blockade for therapeutic purposes.

Therapeutic blockade of inhibitory immune checkpoints is one of the most significant advances in anticancer treatment[1,2]. Monoclonal antibodies that block receptors on T cells (such as PD-1) or their ligands, have shown significant efficacy against various cancer types and have been approved for patient care; however, these agents are not effective against all tumors. This limitation prompted researchers to evaluate other receptors as candidates, including those expressed on innate immune cells[3–9].

Macrophages are components of the innate immune system[4,6,10]. Their main functions are phagocytosis, cytokine production and antigen presentation to T cells. Activation of macrophages is controlled by engagement of various activating and inhibitory receptors, by ligands expressed (or not) on potential 'target' cells. When activating receptors are predominantly triggered, macrophages are activated to display effector functions. Activating receptors include receptors for the Fc portion of antibodies (FcRs), the apoptotic cell receptor MerTK, the integrin CD11b (Mac-1) and the homotypic receptor SLAMF7 (refs. 5,8,10,11); however, when inhibitory receptors are predominantly triggered, macrophage activation is suppressed. The best-studied inhibitory receptor on macrophages is SIRPα, which recognizes as ligand the cell surface molecule CD47, expressed on nearly all normal cells and often overexpressed on tumor cells[3,4,8,9].

There has been increasing interest in blocking SIRPα–CD47 to promote phagocytosis leading to antitumor immunity[5–7,10,12,13]. Blockade of SIRPα–CD47, by CD47 monoclonal antibodies, SIRPα monoclonal antibodies or soluble SIRPα–Fc fusion proteins, has shown promising results in preclinical studies and phase 1/2 clinical trials, in particular against hematological malignancies[5–7,13,14]. The ability of SIRPα–CD47 blockade to augment phagocytosis requires co-engagement of activating receptors, such as FcRs or SLAMF7, by ligands on tumor cells[3–5,8,10,15].

FcRs are engaged when tumor-opsonizing antibodies, such as the therapeutic CD20 monoclonal antibody rituximab, are present[6,10,11]. In contrast, the homotypic receptor SLAMF7 (the ligand of SLAMF7 is another SLAMF7 molecule expressed on another cell) is engaged

[1]Laboratory of Molecular Oncology, Institut de recherches cliniques de Montréal (IRCM), Montréal, Québec, Canada. [2]Department of Medicine, McGill University, Montréal, Québec, Canada. [3]Department of Cell and Developmental Biology, School of Biological Sciences, University of California San Diego, La Jolla, CA, USA. [4]Department of Medicine, University of Montréal, Montréal, Québec, Canada. e-mail: andre.veillette@ircm.qc.ca

https://doi.org/10.1038/s41590-023-01671-2

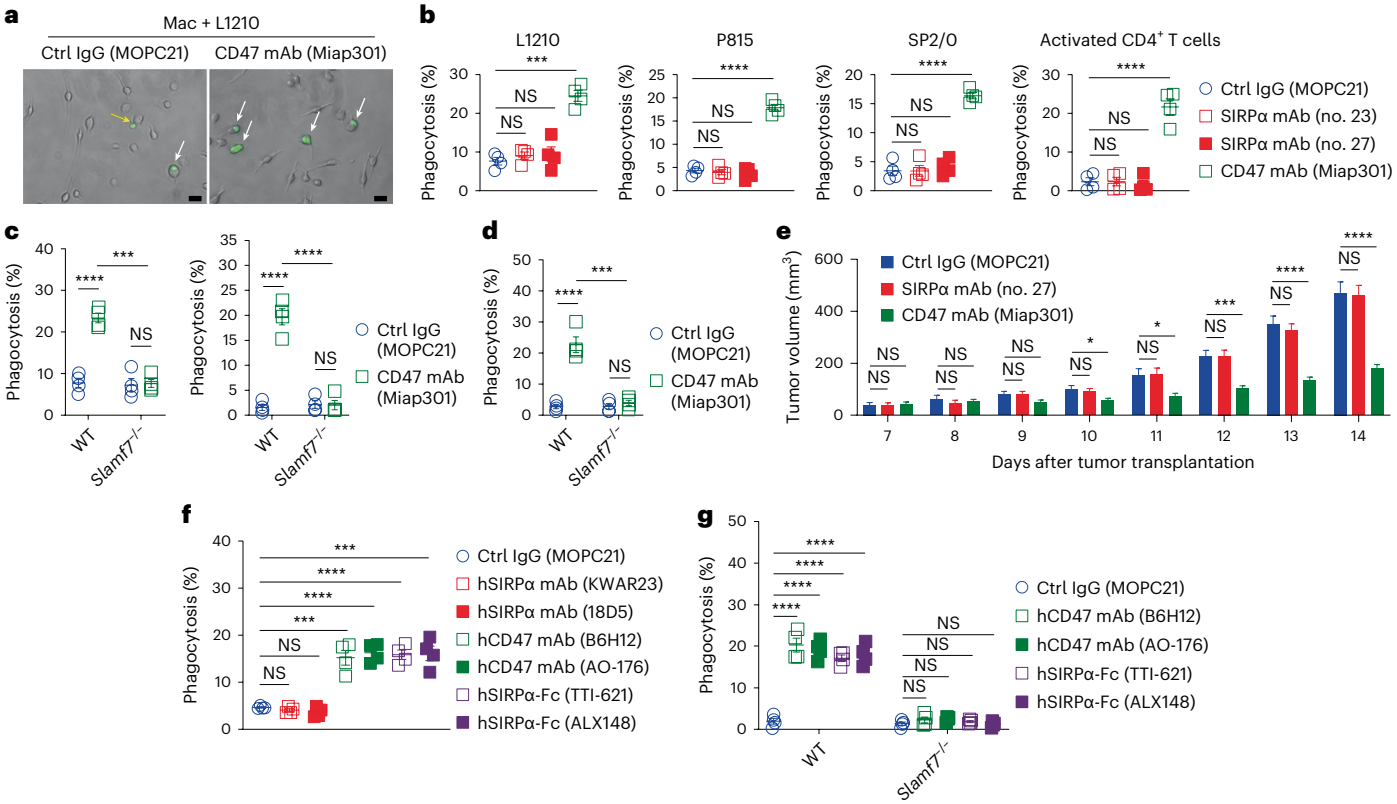

Fig. 1 | CD47, but not SIRPα, inhibits phagocytosis by SLAMF7. **a**,**b**, Representative photomicrographs (**a**) and compiled data from four mice (**b**) of phagocytosis assays of mouse (m) tumor cells L1210, P815, SP2/0 or conA-activated CD4$^+$ T cells by wild-type (WT) BMDMs in the presence of fragment crystallizable (Fc)-silent blocking monoclonal antibodies (mAbs) assayed by fluorescence microscopy. White arrows, phagocytosis of L1210 (green). Yellow arrows, conjugate formation of L1210 with BMDMs without phagocytosis. Scale bars, 50 µm. Mac, macrophage. Ctrl, control. The Fc portion of the mAbs was from mIgG2a and carried the 'LALAPG' mutations, which prevent Fc receptor-binding. **c**, Phagocytosis assays of L1210 cells (left) or conA-activated CD4$^+$ T cells (right) by WT or *Slamf7*$^{-/-}$ BMDMs as in **b**. **d**, Phagocytosis assays of WT or *Slamf7*$^{-/-}$-activated CD4$^+$ T cells by mouse BMDMs, as in **b**. **e**, Tumor volume in *Rag1*$^{-/-}$ mice injected subcutaneously with L1210 cells and with intraperitoneal injection of Fc-silent Ctrl IgG (MOPC21), SIRPα mAb (no. 27) or CD47 mAb (Miap301) on days 7, 8, 9, 10, 11, 12 and 13, measured using a caliper on days 7, 8, 9, 10, 11, 12, 13 and 14. **f**, Phagocytosis assays of human (h) Raji lymphoma cells by human peripheral blood monocyte-derived macrophages in the presence of Fc-silent blocking hSIRPα mAbs KWAR23 and 18D5, hCD47 mAbs B6H12 and AO-176 or soluble fusion proteins TTI-621 and ALX148 were assessed by fluorescence microscopy. The Fc portion from hIgG1 carried the LALAPG mutations. **g**, Phagocytosis of Raji cells by mouse WT or *Slamf7*$^{-/-}$ BMDMs as in **f**. All data are mean ± s.e.m. NS, not significant; $^*P < 0.05$, $^{***}P < 0.001$ and $^{****}P < 0.0001$. Results are representative of four (**a**) independent experiments. Results are pooled from a total of four (**b**–**d**,**g**) mice studied in four (**b**–**d**,**g**) independent experiments; 14 mice from three independent experiments (**e**); and four healthy human donors from four independent experiments (**f**). Each symbol represents one mouse or healthy donor.

when tumor cells express SLAMF7. Among tumors, SLAMF7 is primarily expressed on hematopoietic cancer cells such as multiple myeloma cells and lymphoma cells[4,5,15,16]. SLAMF7-negative tumor cells, such as breast cancer cells, can also be artificially decorated with SLAMF7 using bispecific nanoconjugates, to enable SLAMF7-dependent phagocytosis[17]. The crucial role of SLAMF7 in phagocytosis can be bypassed by activation of the unconventional pro-phagocytic integrins CD11a and CD11c, in response to inflammatory stimuli[15].

One of the limitations of SIRPα–CD47 blockade is that agents blocking CD47 frequently deplete red blood cells and platelets, leading to anemia and thrombocytopenia; agents blocking SIRPα in one study were reported to deplete neutrophils, thus causing neutropenia[3,7,18–20]. Although the mechanisms involved in these toxicities remain to be clarified, neutropenia caused by SIRPα antibodies was dependent on the ability of these agents to engage FcRs. Thus, it is possible that SIRPα–CD47-blocking agents eliminate normal CD47$^+$ or SIRPα$^+$ hematopoietic cells by triggering FcRs. Another possibility is that the blocking agents have yet unappreciated mechanisms of action.

Here we found that, in addition to triggering SIRPα, CD47 suppressed phagocytosis and antitumor immunity by a SIRPα-independent mechanism. This mechanism was the result of a *cis* interaction between CD47 and SLAMF7 on tumor cells, thus preventing the homotypic *trans* interaction of SLAMF7 on tumor cells with SLAMF7 on macrophages. The CD47–SLAMF7 interaction was disrupted by blockade of CD47, but not of SIRPα, and by a first-in-class agonist SLAMF7 antibody. The inhibitory impact of the CD47–SLAMF7 interaction was bypassed when tumor-opsonizing antibodies were present. Hence, CD47 on tumor cells suppressed phagocytosis not only by engaging SIRPα on macrophages, but also by masking tumor cell-intrinsic pro-phagocytic ligands.

Results

CD47, but not SIRPα, inhibits phagocytosis by SLAMF7

To compare the impact of SIRPα and CD47 on phagocytosis, we evaluated side-by-side the effects of previously described or newly generated blocking CD47 monoclonal antibodies, blocking SIRPα monoclonal antibodies or SIRPα fusion proteins, with the latter acting by occupying CD47 on tumor cells. Given the deleterious effects of sustained engagement of FcRs and the tendency to use monoclonal antibodies unable to bind FcRs in the clinic, unless antibody-dependent cellular cytotoxicity or antibody-dependent cellular phagocytosis (ADCP) is attempted[21,22], all agents were engineered to be 'Fc-silent' by including 'LALAPG' mutations in their Fc portion (Extended Data Fig. 1a,b)[23].

https://doi.org/10.1038/s41590-023-01671-2

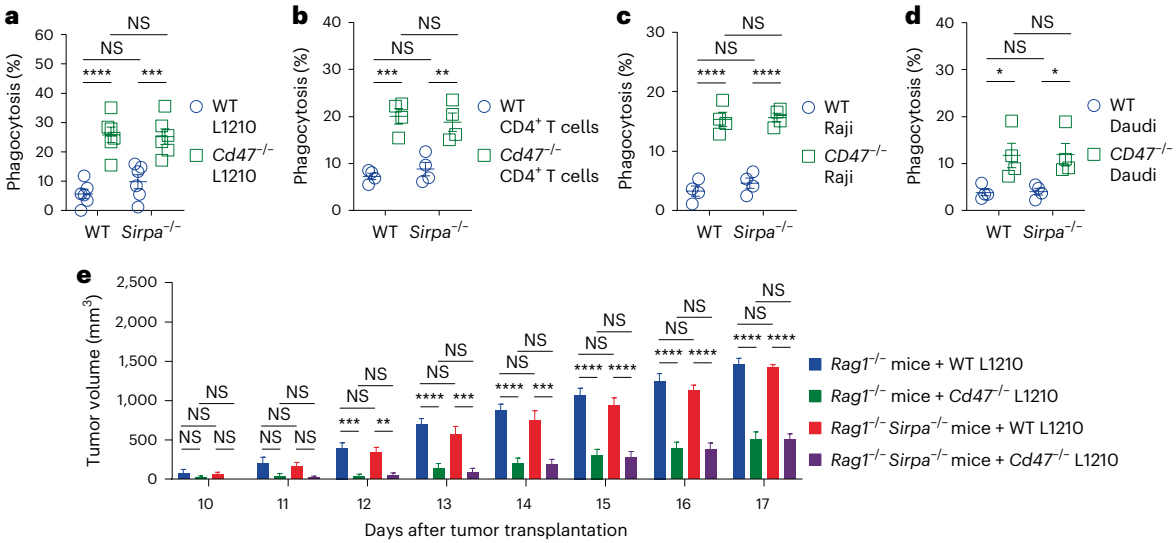

Fig. 2 | Lack of CD47 or SIRPα phenocopies the effects of blockade. **a**–**d**, Phagocytosis of L1210 cells (**a**), conA-activated CD4$^+$ T cells (**b**), Raji cells (**c**) and human lymphoma Daudi cells (**d**), expressing or not expressing CD47, by WT or *Sirpa*$^{-/-}$ BMDMs assayed by fluorescence microscopy. **e**, Tumor volume in *Rag1*$^{-/-}$mice or *Rag1*$^{-/-}$*Sirpa*$^{-/-}$ mice injected subcutaneously with WT L1210 cells and *Cd47*$^{-/-}$ L1210 cells measured using a caliper on days 10, 11, 12, 13, 14, 15, 16 and 17. All data are mean ± s.e.m. *$P < 0.05$, **$P < 0.01$, ***$P < 0.001$ and ****$P < 0.0001$. Results are pooled from six (**a**) or four (**b**–**d**) mice studied in six (**a**) or four (**b**–**d**) independent experiments; 11 (WT L1210) or 10 (*Cd47*$^{-/-}$ L1210) mice from two independent experiments (**e**). Each symbol represents one mouse.

These mutations fully abrogated the ability of monoclonal antibodies to bind FcRs on macrophages (Extended Data Fig. 1b).

When wild-type C57BL/6 mouse bone-marrow-derived macrophages (BMDMs) were used, the blocking mouse CD47 monoclonal antibody Miap301 augmented phagocytosis of the mouse tumor cell lines L1210 (leukemia), P815 (mastocytoma) and SP2/0 (multiple myeloma), compared to the monoclonal antibody MOPC21 used as control (Fig. 1a,b); however, there was no increase in phagocytosis with two newly generated blocking monoclonal antibodies for mouse SIRPα (monoclonal antibodies no. 23 and no. 27) (Fig. 1b and Extended Data Fig. 1c–e). CD47 monoclonal antibodies, but not SIRPα monoclonal antibodies, also promoted phagocytosis of wild-type mouse CD4$^+$ T cells activated by the lectin concanavalin A (conA)[5] (Fig. 1b). These observations were made either with microscopy-based or with pHrodo-based phagocytosis assays (Fig. 1a,b and Extended Data Fig. 2a,b). Similar results were obtained when the CD47 monoclonal antibodies were added only to the target cells or SIRPα monoclonal antibodies were added only to BMDMs, followed by extensive washing to remove unbound antibodies, before phagocytosis (Extended Data Fig. 2c). The ability of CD47 monoclonal antibodies to trigger phagocytosis of L1210 cells and conA-activated CD4$^+$ T cells was abolished using mouse *Slamf7*$^{-/-}$ BMDMs or *Slamf7*$^{-/-}$ T cells (Fig. 1c), confirming the involvement of SLAMF7 (ref. 5). *Slamf7*$^{-/-}$ macrophages were reported to display unaltered FcR-mediated phagocytosis[5]. CD47 monoclonal antibodies, but not SIRPα monoclonal antibodies, also suppressed growth of L1210 cells in a subcutaneous tumor transplantation assay in *Rag1*$^{-/-}$ recipient mice, which lack T cells and B cells, compared to control MOPC21 monoclonal antibodies (Fig. 1e and Extended Data Fig. 2d).

In the human system, blocking human CD47 monoclonal antibodies B6H12 and AO-176, as well as human SIRPα-Fc fusion protein TTI-621 and high-affinity variant ALX148, promoted the phagocytosis of human lymphoma cell line Raji by human blood monocyte-derived macrophages, compared to control MOPC21 monoclonal antibodies (Fig. 1f). The augmented phagocytosis of Raji cells was abolished in mouse *Slamf7*$^{-/-}$ BMDMs compared to wild-type mouse BMDMs (Fig. 1g), indicating that it was SLAMF7-dependent. Mouse SLAMF7, SIRPα and CD47 can interact with human SLAMF7, CD47 and SIRPα, respectively[5]; however, the blocking human SIRPα monoclonal antibodies KWAR23 and 18D5 did not augment phagocytosis by human macrophages (Fig. 1f), and the human SIRPα monoclonal antibodies KWAR23, 18D5, 50A and 40A did not increase phagocytosis by mouse BMDMs ectopically expressing human SIRPα (Extended Data Fig. 2e). Hence, blockade of CD47, but not of SIRPα, promoted in vitro phagocytosis and in vivo elimination of tumor cells expressing the cell-intrinsic pro-phagocytic ligand SLAMF7.

Lack of CD47 or SIRPα phenocopies the effects of blockade

To exclude that the divergent consequences of CD47 and SIRPα blockade were due to differences in the blocking agents, we assessed the impact of loss of CD47 on target cells or SIRPα on macrophages. Wild-type BMDMs showed greater phagocytosis of *Cd47*$^{-/-}$ L1210, *Cd47*$^{-/-}$ conA-activated CD4$^+$ T cells, as well as *CD47*$^{-/-}$ Raji and *CD47*$^{-/-}$ Daudi lymphoma cell lines, compared to their wild-type CD47$^+$ counterparts (Fig. 2a–d and Extended Data Fig. 2f,g); however, compared to wild-type C57BL/6 BMDMs, BMDMs from a newly generated *Sirpa*$^{-/-}$ mouse bred on a pure C57BL/6 background did not exhibit augmented phagocytosis of L1210, conA-activated CD4$^+$ T cells, Raji cells and Daudi cells, when these cells expressed CD47 (Fig. 2a–d and Extended Data Fig. 2f,g). Similar to wild-type BMDMs, *Sirpa*$^{-/-}$ BMDMs showed increased phagocytosis of CD47$^-$ target cells only (Fig. 2a–d and Extended Data Fig. 2f,g). Nonetheless, compared to wild-type BMDMs, *Sirpa*$^{-/-}$ BMDMs displayed increased phagocytosis of CD47$^+$ L1210 cells when BMDMs were pre-treated with the pro-inflammatory stimulus lipopolysaccharide (Extended Data Fig. 2h), which enables phagocytosis through CD18-associated integrins[15]. There was no difference in tumor growth between *Rag1*$^{-/-}$ and *Rag1*$^{-/-}$ *Sirpa*$^{-/-}$ mice, injected subcutaneously with CD47$^-$ or CD47$^+$ L1210 cells (Fig. 2e and Extended Data Fig. 2i).

Sirpa$^{-/-}$ BMDMs had similar RNA sequencing profiles compared to wild-type BMDMs (Extended Data Fig. 3a), suggesting a lack of impact of SIRPα deficiency on macrophage development or differentiation. Moreover, *Sirpa*$^{-/-}$ BMDMs displayed no alteration in cell surface

https://doi.org/10.1038/s41590-023-01671-2

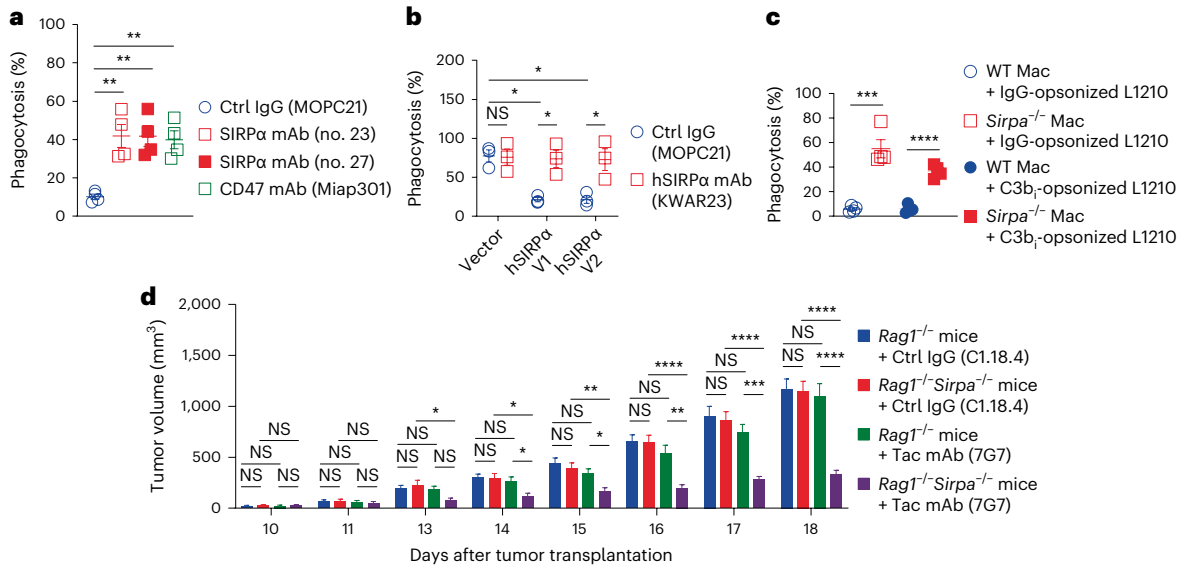

Fig. 3 | Both CD47 and SIRPα inhibit FcR-mediated phagocytosis. **a**, Phagocytosis assays of L1210 derivatives expressing Tac, opsonized with Tac mAb 7G7, which is a mouse IgG2a mAb, by WT BMDMs as in Fig. 1b. **b**, Phagocytosis assays of Raji cells opsonized with hCD20 mAb S18015E, which is a mouse IgG2a mAb, by Sirpα$^{-/-}$ BMDMs expressing the V1 or V2 variant of hSIRPα as in Fig. 1f. **c**, Phagocytosis assays of IgG-opsonized L1210 as in a or L1210 cells opsonized with complement (C3b$_i$) by WT or *Sirpa*$^{-/-}$ BMDMs assayed by fluorescence microscopy. **d**, Tumor volume in *Rag1*$^{-/-}$ mice or *Rag1*$^{-/-}$*Sirpa*$^{-/-}$ mice injected subcutaneously with L1210 derivatives expressing Tac and with intraperitoneal injection of Fc-intact Ctrl IgG C1.18.4 or Tac mAb 7G7 on days 11, 13, 15 and 17, measured using a caliper on days 10, 11, 13, 14, 15, 16, 17 and 18. All data are mean ± s.e.m. $^*P < 0.05$, $^{**}P < 0.01$, $^{***}P < 0.001$ and $^{****}P < 0.0001$. Results are pooled from a total of four (**a**,**c**) or three (**b**) mice studied in four (**a**,**c**) or three (**b**) independent experiments; 15 mice (16 mice in '*Rag1*$^{-/-}$ mice + Tac mAb (7G7)' group) from three independent experiments (**d**). Each symbol represents one mouse.

markers, including SLAMF7 (Extended Data Fig. 3b). Analogous findings were made with a second *Sirpa*$^{-/-}$ C57BL/6 mouse strain (Extended Data Fig. 3c–e). Thus, the loss of CD47 on tumor cells or SIRPα on macrophages mimicked the consequences of antibody blockade.

Both CD47 and SIRPα inhibit FcR-mediated phagocytosis

To ascertain whether the disparate effects of CD47 and SIRPα extended to other pro-phagocytic receptors, tumor cells were 'opsonized' by antibodies (IgG) or complement (C3b$_i$) to trigger FcRs or CD11b (Mac-1), respectively[8]. SIRPα monoclonal antibodies were as efficient as CD47 monoclonal antibodies at augmenting phagocytosis of IgG-opsonized L1210 cells or Raji cells, compared to control MOPC21 monoclonal antibodies (Fig. 3a,b). Similarly, *Sirpa*$^{-/-}$ BMDMs had increased phagocytosis of IgG-opsonized L1210 cells or Raji cells, compared to wild-type BMDMs (Fig. 3c). *Sirpa*$^{-/-}$*Rag1*$^{-/-}$ mice had slower growth of subcutaneously injected Tac$^+$CD47$^+$ L1210 cells compared to *Rag1*$^{-/-}$ mice when injected with Tac monoclonal antibody 7G7, whereas no difference was seen when the mice were injected with the control IgG monoclonal antibody C1.18.4 (Fig. 3d and Extended Data Fig. 4). In vitro, *Sirpa*$^{-/-}$ BMDMs incubated with C3b$_i$-opsonized L1210 cells showed augmented phagocytosis compared to wild-type BMDMs (Fig. 3c). Therefore, blockade or loss of CD47 on target cells and of SIRPα on macrophages were equally efficient at augmenting phagocytosis through FcRs or CD11b.

CD47 interacts in *cis* with SLAMF7 on tumor cells

To explain the inability of blockade or loss of SIRPα to augment phagocytosis of non-opsonized targets, we tested the possibility that CD47 triggered inhibitory receptors other than SIRPα, which could compensate for SIRPα. A soluble CD47–Fc fusion protein had no residual binding to *Sirpa*$^{-/-}$ BMDMs (Fig. 4a), suggesting that this possibility was unlikely. Next, to test the notion that CD47 was disallowing SLAMF7 on tumor cells to trigger SLAMF7 on macrophages by way of a CD47–SLAMF7 *cis* interaction on tumor cells, CD47 was immunoprecipitated from L1210 cells and potential CD47-associated proteins were analyzed by mass spectrometry. As the CD47 monoclonal antibodies targeted the extracellular domain of CD47, we generated L1210 cells expressing a carboxyl-terminal Flag-tagged variant of CD47 and used Flag monoclonal antibodies for CD47 immunoprecipitation (Extended Data Fig. 5a). The amount of Flag-tagged CD47 on these cells was analogous to that of endogenous CD47 on the parental L1210 cells (Extended Data Fig. 5a). Flag-tagged CD47 co-immunoprecipitated with SLAMF7 in the L1210 cells (Fig. 4b and Extended Data Fig. 5b). Several other proteins, such as ribosomal proteins and solute carriers, also co-immunoprecipitated with Flag-tagged CD47 (Fig. 4b and Extended Data Fig. 5b), although less prominently and none represented a known pro-phagocytic ligand. Epitope-tagged CD47 co-immunoprecipitated with SLAMF7 in *CD47*$^{-/-}$ 293T cells transiently transfected with complementary DNAs encoding CD47 and SLAMF7 compared to cells transfected with no cDNA or either cDNA alone (Fig. 4c).

To confirm that CD47 and SLAMF7 were in physical proximity, we conducted fluorescence resonance energy transfer (FRET) studies using *CD47*$^{-/-}$ 293T cells expressing a SNAP-tagged CD47 (SNAP-CD47) labeled with an energy acceptor (Alexa Fluor Dye 647) and CLIP-tagged SLAMF7 (CLIP-SLAMF7) labeled with an energy donor (Dyomics Dye 547) (Fig. 4d,e and Extended Data Fig. 5c). FRET, which reflects a transfer of fluorescence from the donor to the acceptor, can be detected when two molecules are positioned within 10 nm of each other[24]. It is inferred when the fluorescence of the donor is augmented by photobleaching of the acceptor. Photobleaching of Dye 647-labeled SNAP-CD47 resulted in increased fluorescence of Dye 547-labeled CLIP-SLAMF7, compared to the non-photobleached condition (Fig. 4d,e), indicating energy transfer from SLAMF7 to CD47. The FRET was reduced by the CD47 monoclonal antibody Miap301, which interacts with the SIRPα-binding domain of CD47, compared to control MOPC21 monoclonal antibody (Fig. 4d,e). This effect was not due to hindrance with dye labeling by the blocking monoclonal antibodies (Extended Data Fig. 5d). FRET was also diminished by an F37D point mutation in the SIRPα-binding domain of CD47 (hereafter CD47^{F37D}), and by R75A and E77A mutations in the

https://doi.org/10.1038/s41590-023-01671-2

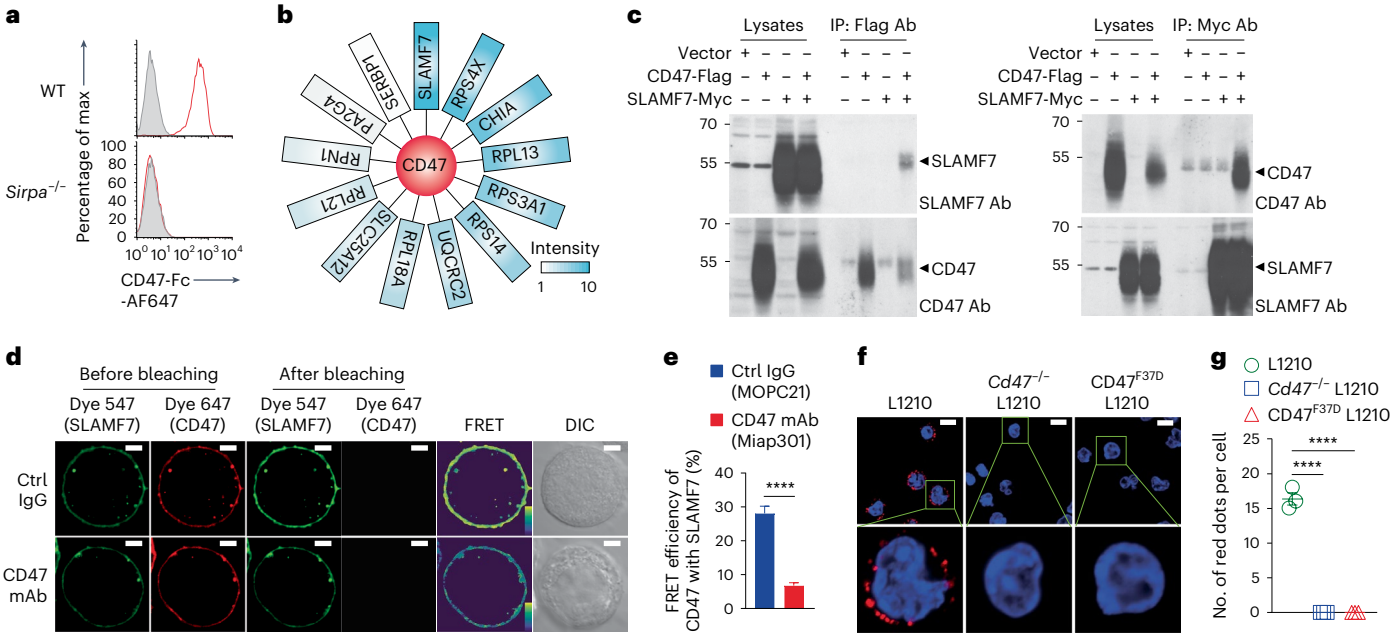

Fig. 4 | CD47 interacts in *cis* with SLAMF7 on tumor cells. a, Binding of CD47-Fc (red line) to WT or *Sirpa*$^{-/-}$ BMDMs assayed by flow cytometry. Filled curves, Ctrl Fc. **b**, Mass spectrometry analysis of Flag mAb immunoprecipitates from L1210 derivatives expressing a Flag-tagged variant of mCD47 showing various potentially associated proteins. **c**, Co-IP assay of CD47 and SLAMF7 in *CD47*$^{-/-}$ 293T cells expressing a Flag-tagged variant of mCD47 and a Myc-tagged variant of mSLAMF7. IP, immunoprecipitation. **d**,**e**, Representative confocal microscopy images (**d**) and compiled data from 18 cells in three independent experiments (**e**) of FRET assays of mCD47 (acceptor) and mSLAMF7 (donor) in *CD47*$^{-/-}$ 293T cells in the presence of Fc-silent Ctrl IgG (MOPC21) or CD47 mAb (Miap301) assayed by confocal microscopy. Pseudo-color, the yellow to purple spectrum denotes strong to weak FRET. Scale bars, 5 µm. **f**,**g**, Representative confocal microscopy images (**f**) and compiled data from three independent experiments (**g**) of PLA assays of mCD47 and mSLAMF7 in L1210 cells, *Cd47*$^{-/-}$ L1210 cells and CD47^{F37D} L1210 cells assayed by confocal microscopy. Scale bar, 10 µm. All data are mean ± s.e.m. ****$P < 0.0001$. Results are representative of five (**a**) or three (**c**,**d**,**f**) independent experiments. Results are pooled from three (**b**,**e**,**g**) independent experiments.

putative self-ligand-binding sequences of SLAMF7 (SLAMF7^{R75A} and SLAMF7^{E77A})[25,26] (Extended Data Fig. 5e–h), indicating that the domains implicated in the CD47–SLAMF7 interaction may be the same as those involved in the CD47–SIRPα and SLAMF7–SLAMF7 interactions. *Cd47*$^{-/-}$ L1210 cells reconstituted with CD47^{F37D} did not repress phagocytosis and, compared to wild-type CD47, CD47^{F37D} did not bind a SIRPα–Fc fusion protein (Extended Data Fig. 6a,b). SLAMF7^{R75A} and SLAMF7^{E77A} did not rescue the pro-phagocytic effect of SLAMF7 when expressed in *Slamf7*$^{-/-}$ conA-activated CD4^{+} T cells, and did not bind to a soluble SLAMF7–Fc fusion protein, compared to wild-type SLAMF7 (Extended Data Figs. 5f and 6c,d), confirming that these mutations abolished the SLAMF7–SLAMF7 interaction.

We also analyzed the proximity of endogenous CD47 and SLAMF7 on L1210 cells using a proximity ligation assay (PLA)[27,28]. PLA can detect proximity of two molecules when they are within 40 nm. After fixing to stabilize proximity, cells were incubated with the CD47 monoclonal antibody Miap301 (modified genetically to possess a mouse IgG2a Fc portion) and SLAMF7 monoclonal antibody 4G2 (modified genetically to possess a human IgG1 Fc portion), followed by oligonucleotide-linked secondary antibodies that specifically recognized the Fc portion of each of the primary antibodies. PCR with complementary oligonucleotides coupled to fluorochromes and fluorescence microscopy detected fluorescent dots in parental L1210 cells, but not in *Cd47*$^{-/-}$ L1210 cells or *Cd47*$^{-/-}$ L1210 cells reconstituted with a CD47^{F37D} mutant (Fig. 4f,g), indicating the presence of CD47–SLAMF7 complexes on L1210 cells.

Finally, to assess whether the physical proximity of CD47 and SLAMF7 was due to a direct interaction, FRET assays were performed using cell-free large unilamellar vesicles (LUVs)[29,30], which were reconstituted with SNAP-Cell-TMR-labeled CD47 and SNAP-Cell-505-labeled SLAMF7 (Extended Data Fig. 6e). Cell-TMR and Cell-505 are the energy acceptor and energy donor, respectively. Addition of SNAP-Cell-TMR-labeled CD47, but not of unrelated SNAP-Cell-TMR-labeled PD-1, quenched the fluorescence of SNAP-Cell-505-labeled SLAMF7 (Extended Data Fig. 6f), indicating energy transfer. The FRET was reduced by the blocking CD47 monoclonal antibody Miap301 or the blocking SLAMF7 monoclonal antibody 4G2 (Extended Data Fig. 6g). Of note, we could not detect binding of a soluble CD47-Fc fusion protein to wild-type or *CD47*$^{-/-}$ Raji cells in vitro (Extended Data Fig. 6h), although Raji cells express SLAMF7 (ref. 5). We postulate that this was due to the fact that the interaction between CD47 and SLAMF7 required that both were positioned within the same cell surface, perhaps in specialized membrane microdomains or structures[31]. Thus, CD47 interacted in *cis* with SLAMF7 at the surface of tumor cells and this interaction was mediated by their canonical ligand-binding domains.

Freeing SLAMF7 from CD47 promotes phagocytosis

To evaluate whether deliverance of SLAMF7 from CD47 was a trigger for phagocytosis, we used two approaches. First, in a binding assay with the BI-141 T cell line ectopically expressing SLAMF7, we observed that blocking CD47 monoclonal antibodies augmented the ability of a soluble SLAMF7–Fc fusion protein to bind to BI-141 cells compared to a control Fc fusion protein (Fig. 5a). Binding of SLAMF7-Fc was not detected on BI-141 cells lacking SLAMF7 (Fig. 5b). Second, we tested whether overexpression of SLAMF7 on tumor cells might create a pool of CD47-free SLAMF7 that could elicit phagocytosis. L1210 cells in which SLAMF7 was overexpressed (~30-fold) were phagocytosed by *Sirpa*$^{-/-}$ BMDMs to nearly the same extent as *Cd47*$^{-/-}$ L1210 cells (Fig. 5c,d). This effect was seen with *Sirpa*$^{-/-}$ BMDMs, but not with *Slamf7*$^{-/-}$*Sirpa*$^{-/-}$ BMDMs (Fig. 5e), confirming that it was mediated by SLAMF7. There was no further increase in phagocytosis by *Sirpa*$^{-/-}$ BMDMs compared to wild-type BMDMs when L1210 target cells lacked

https://doi.org/10.1038/s41590-023-01671-2

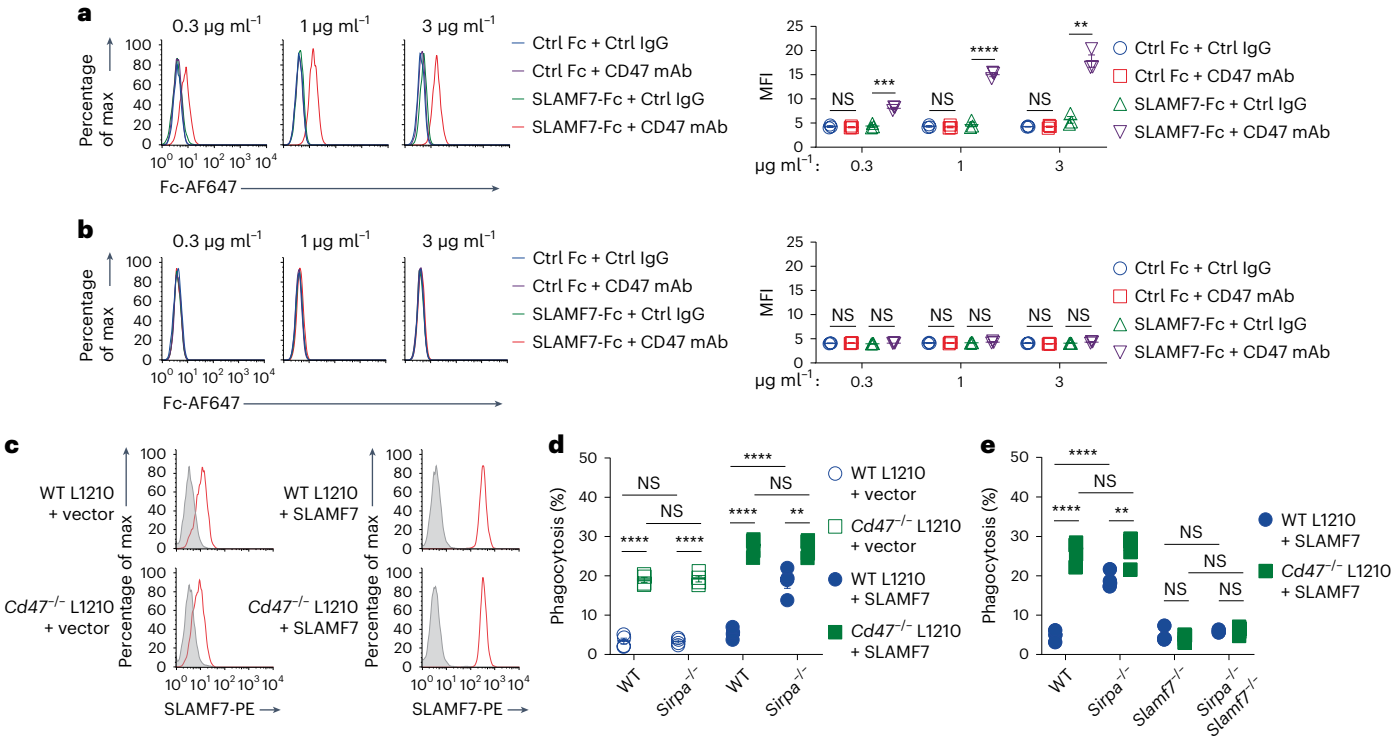

Fig. 5 | Freeing SLAMF7 from CD47 promotes phagocytosis. **a**,**b**, Representative flow cytometry profiles (left) and compiled data from three independent experiments (right) of fusion protein binding assay of 0.3 μg ml^{-1}, 1 μg ml^{-1} or 3 μg ml^{-1} mSLAMF7-Fc to mSLAMF7^{+} (**a**) or mSLAMF7^{-} (**b**) BI-141 tumor cells in the presence of Fc-silent Ctrl IgG (MOPC21) or CD47 mAb (Miap301) assayed by flow cytometry. MFI, mean fluorescence intensity. **c**, Expression of mSLAMF7 (red line) on WT and *Cd47*$^{-/-}$ L1210 cells, with or without mSLAMF7 overexpression, assayed by flow cytometry. Filled curves, Ctrl IgG. **d**, Phagocytosis assays of WT and *Cd47*$^{-/-}$ L1210 cells, with or without mSLAMF7 overexpression, by WT or *Sirpa*$^{-/-}$ BMDMs assayed by fluorescence microscopy. **e**, Phagocytosis assays of WT and *Cd47*$^{-/-}$ L1210 cells, with mSLAMF7 overexpression, by WT, *Sirpa*$^{-/-}$, *Slamf7*$^{-/-}$ or *Sirpa*$^{-/-}$*Slamf7*$^{-/-}$ BMDMs assayed by fluorescence microscopy. All data are mean ± s.e.m. $^{**}P < 0.01$, $^{***}P < 0.001$ and $^{****}P < 0.0001$. Flow cytometry profiles are representative of three (**a**–**c**) independent experiments. Results are pooled from three (**a**,**b**) independent experiments; four (**d**,**e**) mice studied in four (**d**,**e**) independent experiments. Each symbol represents one mouse.

CD47 and overexpressed SLAMF7 (Fig. 5d,e). These data suggested that the release of SLAMF7 from CD47 by blocking CD47 monoclonal antibodies or enforced expression of SLAMF7 promoted phagocytosis.

A first-in-class SLAMF7 monoclonal antibody Z10 promotes phagocytosis

To test further if interference with the SLAMF7-CD47 interaction triggered phagocytosis, we screened for pro-phagocytic SLAMF7 monoclonal antibodies that would block this interaction. We generated a large collection of mouse monoclonal antibodies reacting with human SLAMF7 and also tested elotuzumab, a non-blocking SLAMF7 monoclonal antibody used for the treatment of multiple myeloma[32]. All monoclonal antibodies reacted with human, but not mouse, SLAMF7, and were modified to be Fc-silent hIgG1 (Methods). One of the newly generated monoclonal antibodies, Z10, stimulated the phagocytosis of Raji cells by *Sirpa*$^{-/-}$ mouse BMDMs, but not by wild-type BMDMs, compared to all other monoclonal antibodies tested, including elotuzumab (Fig. 6a,b). The combined impact of Z10 and SIRPα deficiency on phagocytosis was analogous to that of the CD47 monoclonal antibody B6H12 (Fig. 6a). In addition, Z10 triggered the ability of *Sirpa*$^{-/-}$ BMDMs to phagocytose Daudi cells and the multiple myeloma cell line MM.1S, which express human SLAMF7 endogenously and Fc-silent CD3 + CD28 monoclonal antibody-activated mouse CD8^{+} T cells transduced with human SLAMF7 (Extended Data Fig. 7a,b). It also increased phagocytosis of Raji cells by human blood monocyte-derived macrophages, or by mouse BMDMs retrovirally transduced with human SLAMF7, compared to control MOPC21 monoclonal antibodies (Fig. 6c–e). Z10 had no impact when using mouse BMDMs that expressed human SLAMF7 and L1210 target cells that expressed endogenous mouse SLAMF7 (Fig. 6f and Extended Data Fig. 7c), indicating that the pro-phagocytic effect of Z10 required human SLAMF7 on the target cells.

In *Rag1*$^{-/-}$ mice subcutaneously injected with Raji cells, intraperitoneal co-administration of the SIRPα monoclonal antibody no. 27 and Z10 suppressed tumor growth and increased survival more than CD47 monoclonal antibody B6H12 compared to control MOPC21 IgG (Fig. 6g,h and Extended Data Fig. 7d). No antitumor effect was seen with SIRPα monoclonal antibody no. 27 alone, Z10 alone, SIRPα monoclonal antibody no. 27 + elotuzumab or elotuzumab alone (Fig. 6g and Extended Data Fig. 7d). Thus, Z10 is an agonist monoclonal antibody that stimulated phagocytosis and prevented tumor growth when combined with SIRPα blockade, an impact that required Z10 binding to SLAMF7 on tumor cells, not on macrophages.

Monoclonal antibody Z10 frees SLAMF7 from CD47

Using FRET assays performed in transfected 293T cells, we observed that either Z10 or the CD47 monoclonal antibody B6H12, but not elotuzumab, dissociated the *cis* interaction between CD47 and SLAMF7 (Fig. 7a,b). Z10 also disrupted the co-immunoprecipitation of CD47 and SLAMF7 in 293T cells (Extended Data Fig. 8a). In confocal microscopy analyses, Z10, but not control MOPC21 monoclonal antibody, enhanced actin polarization in *Sirpa*$^{-/-}$ BMDMs exposed to L1210 tumor cells, without promoting conjugate formation between macrophages and tumor cells, as reported for CD47 monoclonal antibody Miap301 (ref. 5) (Fig. 7c and Extended Data Fig. 8b,c). To examine whether Z10 targeted

https://doi.org/10.1038/s41590-023-01671-2

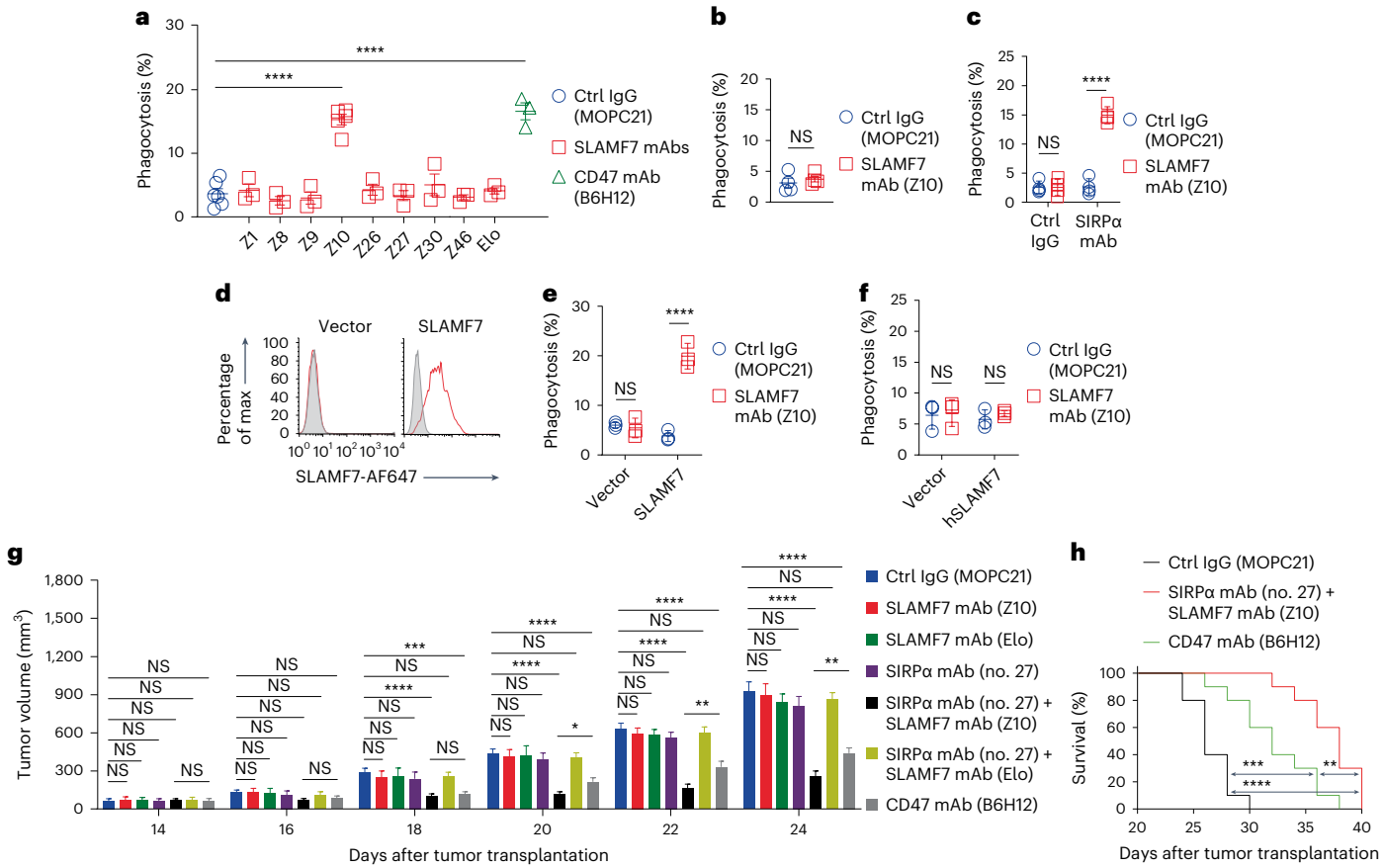

Fig. 6 | First-in-class SLAMF7 mAb Z10 promotes phagocytosis. **a**,**b**, Phagocytosis of Raji cells by *Sirpa*$^{-/-}$ (**a**) or WT (**b**) BMDMs as in Fig. 1f. Elo, elotuzumab. **c**, Phagocytosis assays of Raji cells by human peripheral blood monocyte-derived macrophages as in Fig. 1f. **d**, Expression of hSLAMF7 (red line) in SFR KO *Sirpa*$^{-/-}$ BMDMs, expressing or not expressing hSLAMF7, assayed by flow cytometry. Filled curves, Ctrl IgG. **e**,**f**, Phagocytosis assays of human Raji cells (**e**) or mouse L1210 cells (**f**) by SFR KO *Sirpa*$^{-/-}$ BMDMs, expressing or not expressing hSLAMF7, as in Fig. 1f. **g**, Tumor volume in *Rag1*$^{-/-}$ mice injected subcutaneously with Raji cells, and with intraperitoneal injection of Fc-silent mAbs on days 14, 16, 18, 20 and 22, measured using a caliper on days 14, 16, 18, 20, 22 and 24. **h**, Survival curves of *Rag1*$^{-/-}$ mice injected subcutaneously with Raji cells, and with intraperitoneal injection of Fc-silent mAbs on days 14, 16, 18, 20 and 22. All data are mean ± s.e.m. *$P < 0.05$, **$P < 0.01$, ***$P < 0.001$ and ****$P < 0.0001$. Flow cytometry profiles are representative of three (**d**) independent experiments. Results are pooled from three (**a**, except six for Ctrl IgG and five for Z10) (**e**,**f**) or four (**b**) mice studied in six (**a**), three (**e**,**f**) or four (**b**) independent experiments; four healthy human donors from four independent experiments (**c**); 18 mice ('Ctrl IgG (MOPC21)', 'SIRPα mAb (no. 27) + SLAMF7 mAb (Z10)' and 'CD47 mAb (B6H12)' groups) from four independent experiments, eight mice ('SLAMF7 mAb (Elo) and 'SIRPα mAb (no. 27) + SLAMF7 mAb (Elo)' groups) and seven mice ('SLAMF7 mAb (Z10)' and 'SIRPα mAb (no. 27)' groups) from two independent experiments (**g**); ten mice from two independent experiments (**h**). Each symbol represents one mouse or healthy donor.

epitopes directly involved in SLAMF7–SLAMF7 or CD47–SLAMF7 interactions, we first analyzed its binding to chimeric SLAMF7 molecules bearing the first Ig-like domain (Ig(V)) of mouse SLAMF7 and the second Ig-like domain (Ig(C)) of human SLAMF7 and vice versa, named mSLAMF7(V)-hSLAMF7(C) and hSLAMF7(V)-mSLAMF7(C), respectively. Similar to elotuzumab, Z10 interacted with mSLAMF7(V)-hSLAMF7(C), but not hSLAMF7(V)-mSLAMF7(C) (Fig. 7d), implying that it bound to the second Ig-like domain of hSLAMF7, which is not directly involved in the SLAMF7–SLAMF7 interaction. In contrast, another SLAMF7 monoclonal antibody, Z8, interacted with the first Ig-like domain of SLAMF7, which is needed for the homotypic interaction (Fig. 7d). Z10 did not interfere with the phagocytosis of *CD47*$^{-/-}$ Raji cells or *CD47*$^{-/-}$ Daudi cells, which are phagocytosed through SLAMF7 (Extended Data Fig. 9a,b), further indicating that Z10 did not target epitopes involved in the SLAMF7–SLAMF7 interaction. Replacement of amino acids 169–176 or 181–188 in human SLAMF7 by the equivalent mouse sequences abolished binding by Z10 and elotuzumab, but not by Z8 (Extended Data Fig. 10a). The introduction of single point mutations in human SLAMF7 further indicated that arginine 181 (R181), asparagine 182 (N182), phenylalanine 183 (F183) or, to a lesser extent, valine 174 (V174) were needed for binding by Z10 and elotuzumab, but not by monoclonal antibody Z8 (Fig. 7e and Extended Data Fig. 10b). Compared to elotuzumab, V174 and N182 were more critical for Z10 binding (Fig. 7e and Extended Data Fig. 10b), suggesting differences in the binding mechanisms of Z10 and elotuzumab. Mutation in amino acids 172, 173 or 177 abolished or greatly reduced Z10, elotuzumab and Z8 binding (Extended Data Fig. 10b), indicating that these mutations likely compromised expression of SLAMF7 at the cell surface. As such, Z10 dissociated the CD47–SLAMF7 *cis* interaction on tumor cells, without interacting with sequences directly involved in the SLAMF7–SLAMF7 interaction, suggesting that the effect of Z10 was due to conformational modification of SLAMF7 rather than direct blocking of CD47–SLAMF7, which seemingly implicated sequences similar to those involved in the SLAMF7–SLAMF7 interaction.

Discussion

In this report, we have identified a mechanism by which CD47 prevents phagocytosis. In addition to its ability to trigger SIRPα on macrophages, CD47 on tumor cells physically interacted in *cis* with SLAMF7, thereby masking the ability of this ligand to engage its receptor on macrophages

https://doi.org/10.1038/s41590-023-01671-2

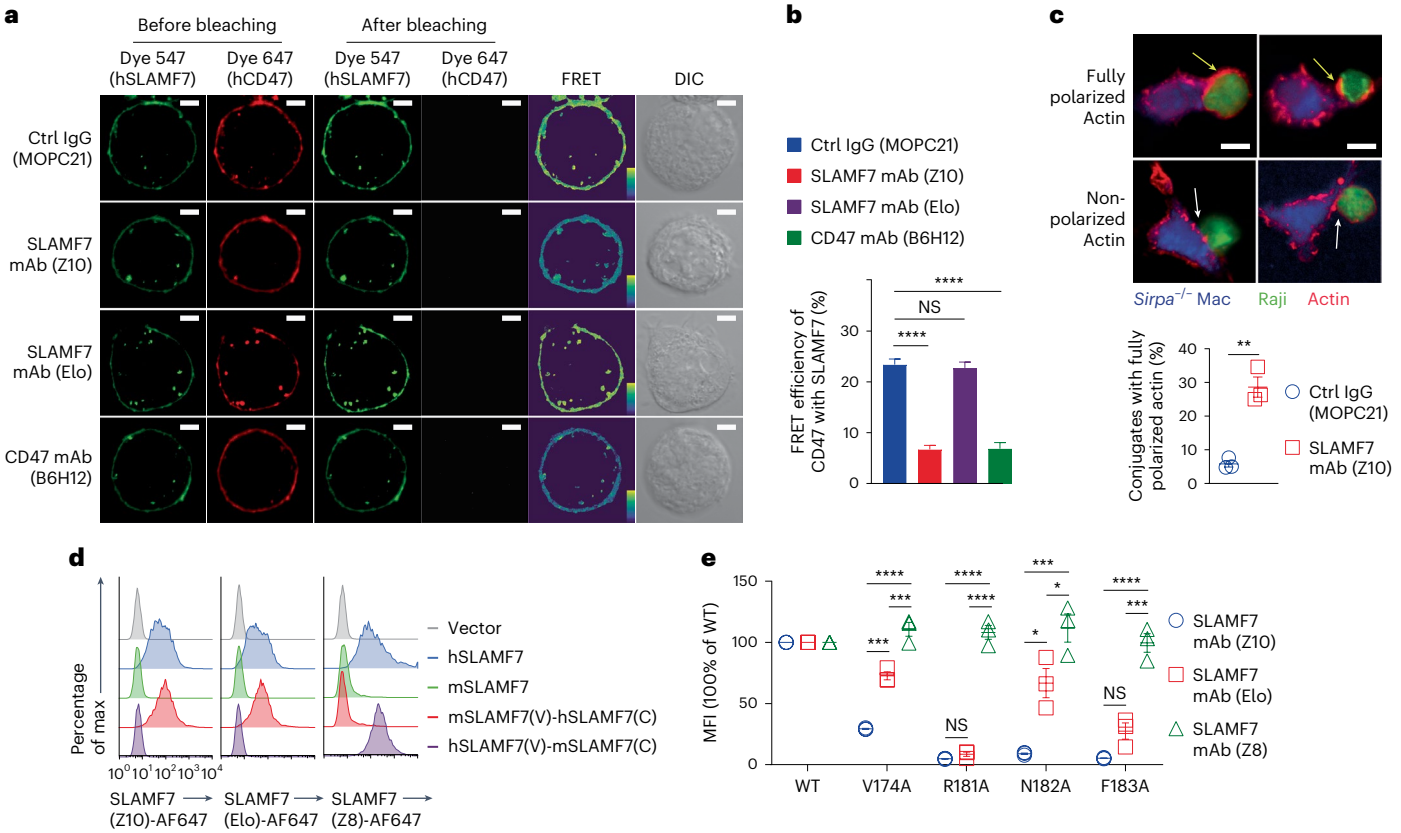

Fig. 7 | mAb Z10 frees SLAMF7 from CD47. a,**b**, Representative confocal microscopy images (**a**) and compiled data from 18 cells in three independent experiments (**b**) of FRET assays of hCD47 (acceptor) and hSLAMF7 (donor) as in Fig. 4d,e. **c**, Representative confocal microscopy images (top) and compiled data from three independent experiments (bottom) of Actin polarization assays in co-culture of *Sirpa*$^{-/-}$ BMDMs and L1210 cells assessed by confocal microscopy. Yellow arrows, fully polarized actin. White arrows, nonpolarized Actin. Scale bars, 5 µm. **d**, Binding of hSLAMF7 mAbs Z10, Elo and Z8 to *CD47*$^{-/-}$ 293T cells expressing hSLAMF7, mSLAMF7 or chimeras between hSLAMF7 and mSLAMF7 assayed by flow cytometry. V, variable Ig-like. C, constant Ig-like. **e**, binding of hSLAMF7 mAbs Z10, Elo and Z8 to *CD47*$^{-/-}$ 293T cells expressing hSLAMF7, hSLAMF7^{V174A}, hSLAMF7^{R181A}, hSLAMF7^{N182A} or hSLAMF7^{F183A} assayed by flow cytometry. All data are mean ± s.e.m. *$P < 0.05$, **$P < 0.01$, ***$P < 0.001$ and ****$P < 0.0001$. Photographs are representative of three (**a**,**c**) independent experiments. Flow cytometry profiles are representative of six (**d**, except two for mSLAMF7) independent experiments. Results are pooled from three (**b**,**c**,**e**) independent experiments. Each symbol represents one mouse.

to trigger phagocytosis. Relief of both mechanisms was needed for phagocytosis of tumor cells, unless the SIRPα-independent mechanism was bypassed by antibodies or complement, or by inflammatory stimuli.

We postulate that the high efficiency by which CD47 suppressed the function of SLAMF7 was due to the fact that CD47 was much more abundant than SLAMF7 on target cells. Hence, it easily saturated all ligand-binding surfaces on SLAMF7. This interpretation was consistent with the observation that L1210 cells that overexpressed SLAMF7 had augmented phagocytosis and is supported by published quantitative proteomic analyses, whereby CD47 was estimated to be ~tenfold more abundant than SLAMF7 in activated T cells[33].

The only known pro-phagocytic ligand that co-immunoprecipitated with CD47 in L1210 cells was SLAMF7. Nevertheless, it is possible that CD47 also interacts in *cis* with other pro-phagocytic ligands. For instance, CD47 may associate with ligands on red blood cells and platelets, which are depleted during CD47 blockade and lack SLAMF7 (refs. 3,7,18–20). Although removal of these cells during CD47 blockade may be mediated through engagement of FcRs by the Fc portion of CD47 monoclonal antibodies or SIRPα–Fc fusion proteins, it is plausible that CD47 blockade unmasks pro-phagocytic ligands on these cells. Future studies addressing these possibilities may help design strategies to attenuate the toxicities of SIRPα–CD47 blockade.

The *cis* interaction between CD47 and SLAMF7 seemingly involved the ligand-binding domains implicated in the *trans* interactions with SIRPα and SLAMF7, respectively. Accordingly, the CD47–SLAMF7 association was relieved by blocking CD47 monoclonal antibodies, but not by blocking SIRPα monoclonal antibodies. The CD47–SLAMF7 association was also alleviated by Z10, which seemed to act by conformational modification of SLAMF7. Given that both CD47 and SLAMF7 are members of the immunoglobulin superfamily, which encompasses several proteins capable of heterotypic interactions, and given the results of our PLA and LUV assays, we posit that the CD47–SLAMF7 association was direct; however, formal demonstration of this notion will require structural studies.

Although Z10 had no appreciable single-agent antitumor activity, it enabled tumor cell elimination in vitro and in vivo when combined with SIRPα blockade, suggesting an effective new combination therapy against SLAMF7^{+} malignancies, such as multiple myeloma and lymphoma. This antitumor effect was not observed with elotuzumab. In *Rag1*$^{-/-}$ mice inoculated with human lymphoma B cells (Raji cells), Z10 + SIRPα blockade was more effective at suppressing tumor growth than CD47 blockade. Although this difference remains to be confirmed using other tumor models and in the clinic, one possibility is that the higher expression of CD47 on tumor cells, in addition to the large 'sink' of CD47 on normal cells in humans, would make CD47 more difficult to saturate with antibodies than SIRPα and SLAMF7 in patients with cancer. For the same reasons, SIRPα blockade may also be preferable to CD47 blockade in combinations using tumor-opsonizing monoclonal antibodies to trigger ADCP. Another advantage of Z10 + SIRPα blockade over CD47 blockade is that red blood cells and platelets would be spared

by this combination, although it may not be the case for activated T cells, which express SLAMF7.

BMDMs from our *Sirpa*$^{-/-}$ mouse strain, which was created in the C57BL/6 background, did not show an altered transcriptional profile compared to wild-type BMDMs. Splenic macrophages from a distinct *Sirpa*$^{-/-}$ mouse strain on a mixed C3H/HeN-C57BL/6 background were reported to have changes in messenger RNA expression compared to wild-type BMDMs[34]. The basis for this discrepancy remains to be clarified, but it may reflect the use of different types of macrophages, or differences in genetic background or microbiome between the two mouse strains.

In addition to enhancing our comprehension of how CD47 prevents phagocytosis and to providing insights into the relative advantages of targeting SIRPα versus CD47 for therapeutic purposes, these results exemplified the notion that blockade of receptors and blockade of their ligands do not always have the same impact. This dichotomy can translate into differences in therapeutic efficacy and toxicity. Such a phenomenon occurs because receptors and their ligands can have partially divergent mechanisms of action. A better knowledge of how receptors and ligands work is crucial for making the best decisions regarding which ones to target in therapies of human diseases.

Online content

Any methods, additional references, Nature Portfolio reporting summaries, source data, extended data, supplementary information, acknowledgements, peer review information; details of author contributions and competing interests; and statements of data and code availability are available at https://doi.org/10.1038/s41590-023-01671-2.

References

1. Minn, A. J. & Wherry, E. J. Combination cancer therapies with immune checkpoint blockade: convergence on interferon signaling. *Cell* **165**, 272–275 (2016).
2. Sharma, P. & Allison, J. P. Dissecting the mechanisms of immune checkpoint therapy. *Nat. Rev. Immunol.* **20**, 75–76 (2020).
3. Son, J. et al. Inhibition of the CD47-SIRPα axis for cancer therapy: a systematic review and meta-analysis of emerging clinical data. *Front. Immunol.* **13**, 1027235 (2022).
4. Veillette, A. & Chen, J. SIRPα-CD47 immune checkpoint blockade in anticancer therapy. *Trends Immunol.* **39**, 173–184 (2018).
5. Chen, J. et al. SLAMF7 is critical for phagocytosis of haematopoietic tumour cells via Mac-1 integrin. *Nature* **544**, 493–497 (2017).
6. Chao, M. P. et al. Anti-CD47 antibody synergizes with rituximab to promote phagocytosis and eradicate non-Hodgkin lymphoma. *Cell* **142**, 699–713 (2010).
7. Advani, R. et al. CD47 blockade by Hu5F9-G4 and rituximab in non-Hodgkin's lymphoma. *N. Engl. J. Med.* **379**, 1711–1721 (2018).
8. Feng, M. et al. Phagocytosis checkpoints as new targets for cancer immunotherapy. *Nat. Rev. Cancer* **19**, 568–586 (2019).
9. Matlung, H. L., Szilagyi, K., Barclay, N. A. & van den Berg, T. K. The CD47–SIRPα signaling axis as an innate immune checkpoint in cancer. *Immunol. Rev.* **276**, 145–164 (2017).
10. Zhao, X. W. et al. CD47-signal regulatory protein-α (SIRPα) interactions form a barrier for antibody-mediated tumor cell destruction. *Proc. Natl Acad. Sci. USA* **108**, 18342–18347 (2011).
11. Zhao, X. W., Kuijpers, T. W. & van den Berg, T. K. Is targeting of CD47–SIRPα enough for treating hematopoietic malignancy? *Blood* **119**, 4333–4334 (2012).
12. Petrova, P. S. et al. TTI-621 (SIRPαFc): a CD47-blocking innate immune checkpoint inhibitor with broad antitumor activity and minimal erythrocyte binding. *Clin. Cancer Res.* **23**, 1068–1079 (2017).
13. Weiskopf, K. et al. Engineered SIRPα variants as immunotherapeutic adjuvants to anticancer antibodies. *Science* **341**, 88–91 (2013).
14. Ring, N. G. et al. Anti-SIRPα antibody immunotherapy enhances neutrophil and macrophage antitumor activity. *Proc. Natl Acad. Sci. USA* **114**, E10578–E10585 (2017).
15. Tang, Z. et al. Inflammatory macrophages exploit unconventional pro-phagocytic integrins for phagocytosis and anti-tumor immunity. *Cell Rep.* **37**, 110111 (2021).
16. Guo, H., Cruz-Munoz, M. E., Wu, N., Robbins, M. & Veillette, A. Immune cell inhibition by SLAMF7 is mediated by a mechanism requiring src kinases, CD45, and SHIP-1 that is defective in multiple myeloma cells. *Mol. Cell. Biol.* **35**, 41–51 (2015).
17. Lu, Y. et al. Immunological conversion of solid tumours using a bispecific nanobioconjugate for cancer immunotherapy. *Nat. Nanotechnol*. https://doi.org/10.1038/s41565-022-01245-7 (2022).
18. Johnson, L. D. S. et al. Targeting CD47 in Sezary syndrome with SIRPαFc. *Blood Adv.* **3**, 1145–1153 (2019).
19. Querfeld, C. et al. Intralesional TTI-621, a novel biologic targeting the innate immune checkpoint CD47, in patients with relapsed or refractory mycosis fungoides or Sezary syndrome: a multicentre, phase 1 study. *Lancet Haematol.* **8**, e808–e817 (2021).
20. Strati, P. et al. Interim results from the first clinical study of CC-95251, an anti-signal regulatory protein-α (SIRPα) antibody, in combination with rituximab in patients with relapsed and/or refractory non-Hodgkin lymphoma (R/R NHL). *Blood* **138**, 2493 (2021).
21. Delidakis, G., Kim, J. E., George, K. & Georgiou, G. Improving antibody therapeutics by manipulating the Fc domain: immunological and structural considerations. *Annu. Rev. Biomed. Eng.* **24**, 249–274 (2022).
22. Kang, T. H. & Jung, S. T. Boosting therapeutic potency of antibodies by taming Fc domain functions. *Exp. Mol. Med.* **51**, 1–9 (2019).
23. Lo, M. et al. Effector-attenuating substitutions that maintain antibody stability and reduce toxicity in mice. *J. Biol. Chem.* **292**, 3900–3908 (2017).
24. Sekar, R. B. & Periasamy, A. Fluorescence resonance energy transfer (FRET) microscopy imaging of live cell protein localizations. *J. Cell Biol.* **160**, 629 (2003).
25. Cao, E. et al. NTB-A receptor crystal structure: insights into homophilic interactions in the signaling lymphocytic activation molecule receptor family. *Immunity* **25**, 559–570 (2006).
26. Hatherley, D. et al. Paired receptor specificity explained by structures of signal regulatory proteins alone and complexed with CD47. *Mol. Cell* **31**, 266–277 (2008).
27. Goyette, M.-A. et al. The receptor tyrosine kinase AXL is required at multiple steps of the metastatic cascade during HER2-positive breast cancer progression. *Cell Rep.* **23**, 1476–1490 (2018).
28. Blanchard, E. L. et al. Proximity ligation assays for in situ detection of innate immune activation: focus on in vitro-transcribed mRNA. *Mol. Ther. Nucleic Acids* **14**, 52–66 (2019).
29. Zhao, Y. et al. Antigen-presenting cell-intrinsic PD-1 neutralizes PD-L1 in *cis* to attenuate PD-1 signaling in T cells. *Cell Rep.* **24**, 379–390 (2018).
30. Zhao, Y. et al. PD-L1:CD80 *cis*-heterodimer triggers the co-stimulatory receptor CD28 while repressing the inhibitory PD-1 and CTLA-4 pathways. *Immunity* **51**, 1059–1073 (2019).
31. Zhao, Y. et al. cis-B7: CD28 interactions at invaginated synaptic membranes provide CD28 co-stimulation and promote CD8^{+} T cell function and anti-tumor immunity. *Immunity* https://doi.org/10.1016/j.immuni.2023.04.005 (2023).
32. Ritchie, D. & Colonna, M. Mechanisms of action and clinical development of elotuzumab. *Clin. Transl. Sci.* **11**, 261–266 (2018).

33. Howden, A. J. M. et al. Quantitative analysis of T cell proteomes and environmental sensors during T cell differentiation. *Nat. Immunol.* **20**, 1542–1554 (2019).
34. Bian, Z. et al. Cd47-Sirpα interaction and IL-10 constrain inflammation-induced macrophage phagocytosis of healthy self-cells. *Proc. Natl Acad. Sci. USA* **113**, E5434–E5443 (2016).

Methods

Mice

Mice lacking SIRPα (*Sirpa*$^{-/-}$) were generated in our laboratory using fertilized C57BL/6J oocytes and CRISPR-Cas-based genomic editing. The following guide RNAs were used: 5′- AGCAGCGGCCC TAGGCGGCC-3′, 5′-GCCCGGCCCCTGGCCGCCTA-3′ and 5′- TCCGCG TCCTGTTTCTGTAC-3′. After birth, mice were screened by flow cytometry and sequencing of the *Sirpa* gene. Strains bearing a 593-nucleotide (no. 46) or 11-nucleotide (no. 54) deletion in exon 2 of *Sirpa* were chosen. These deletions resulted in a frameshift in the second coding exon of the *Sirpa* gene and caused loss of SIRPα expression by flow cytometry. Heterozygous *Sirpa*$^{+/-}$ mice were backcrossed to the C57BL/6J background for more than ten generations and subsequently bred to homozygosity for experimentation. The no. 46 mouse strain was used for most experiments, unless specified. Mice lacking all SFRs (SFR KO) or SLAMF7 (*Slamf7*$^{-/-}$), and mice expressing a human (h) *SLAMF7* bacterial artificial chromosome transgene (*hSLAMF7* BAC Tg mice), in the C57BL/6J background, were described elsewhere[5,35]. *Cd47*$^{-/-}$, *Rag1*$^{-/-}$ and C57BL/6J mice were obtained from the Jackson Laboratory. *Sirpa*$^{-/-}$ mice were bred with SFR KO or *Slamf7*$^{-/-}$ mice to create SFR KO *Sirpa*$^{-/-}$ mice and *Sirpa*$^{-/-}$ *Slamf7*$^{-/-}$ mice. *hSLAMF7* BAC Tg mice were bred with *Slamf7*$^{-/-}$ mice to create *Slamf7*$^{-/-}$*hSLAMF7* BAC Tg mice. *Rag1*$^{-/-}$ *Sirpa*$^{-/-}$ mice were generated in the same manner as *Sirpa*$^{-/-}$ mice, except that *Rag1*$^{-/-}$ oocytes were used for micro-injection of guide RNAs. This approach was needed because the *Sirpa* and *Rag1* genes are located closely on the same chromosome. A mouse strain bearing a 168-nucleotide deletion in exon 2 of *Sirpa* was chosen. This deletion resulted in a frameshift in the second coding exon of the *Sirpa* gene and caused loss of SIRPα expression by flow cytometry.

All mice were maintained in the C57BL/6J background. They were kept in a specific-pathogen-free environment. Either males or females were used, between 8 to 12 weeks of age. Littermates were used as control in most experiments, except for some studies where WT syngeneic, age and sex-matched mice were used. Animal experimentation was performed in accordance to the Canadian Council of Animal Care and approved by the IRCM Animal Care Committee.

Cells

Macrophages were generated as described[5]. Briefly, for mouse macrophages, BMDMs were generated by growing freshly isolated bone-marrow cells for 7 d in medium supplemented with 30% (*v*/*v*) L929 cell-conditioned medium as a source of colony-stimulating factor (CSF)-1. Human macrophages were produced from peripheral blood mononuclear cells, which were isolated from healthy donors using Ficoll-Paque PLUS (cat. no. 36-101-6383, GE Healthcare), according to the manufacturer's protocol and as approved by the IRCM Human Ethics Board. Peripheral blood mononuclear cells were then seeded onto Petri dishes containing serum-free RPMI medium for 30 min. After gentle washes to remove non-adherent cells, adherent cells (which mostly represent monocytes) were differentiated into macrophages by culture in medium supplemented with 10% human serum and 10 ng ml^{-1} CSF-1 (cat. no. 300-25, Peprotech) for 7 d.

Mouse CD4$^+$ or CD8$^+$ T cells, depleted of natural killer (NK) T cells using NK1.1 monoclonal antibody, were purified from spleen by negative selection using the EasySep Purification kits (cat. no. 19852 or 19853, STEMCELL Technologies). Activated CD4$^+$ T cells were obtained by stimulating CD4$^+$ T cells with 4 µg ml^{-1} conA (cat. no. C5275, Sigma-Aldrich) for 2 d, followed by expansion for 3 d in medium containing 50 U ml^{-1} IL-2 (cat. no. 212-12, Peprotech). Activated CD8$^+$ T cells were obtained by stimulating CD8$^+$ T cells with 3 µg ml^{-1} Fc-silent CD3 monoclonal antibody (145-2C11, Absolute Biotech Company) plus 1 µg ml^{-1} Fc-silent CD28 monoclonal antibody (D665, Absolute Biotech Company) for 2 d.

L1210 (CCL-219), P815 (TIB-64), SP2/0 (CRL-1581), Raji (CCL-86), Daudi (CCL-213), MM.1S (CRL-2974), L929 (CCL-1), EL-4 (TIB-39), FO (CRL-1646), 293T (CRL-3216) and Phoenix-Eco (CRL-3214) were obtained from The American Type Culture Collection. The T cell hybridoma line BI-141 was reported elsewhere[36]. Immune cells were authenticated by the provider and verified by flow cytometry. All cells were negative for *Mycoplasma*.

CRISPR-Cas9 knockout and retroviral infection

Cd47$^{-/-}$ L1210 cells and *CD47*$^{-/-}$ 293T cells were generated by CRISPR-Cas-mediated genome editing, using plasmid PX458 (cat. no. 48138, Addgene) and the following guide RNAs: mouse *Cd47*: 5′-CACCGAGCAACAGCGCCGCCGCCAA-3′ and 5′-CACCGTTGGCG GCGGCGCTGTTGCT-3′; human *CD47*: 5′-CTGGTAGCGGCGCTG TTGCT-3′. *CD47*$^{-/-}$ Raji cells and *CD47*$^{-/-}$ Daudi cells were generated using the Neon Transfection System kit (cat. no. MPK10096, Thermo Fisher Scientific), guide RNA 5′-CTACTGAAGTATACGTAAAG-3′ or scrambled guide RNA (cat. no. 1072544, IDT) and the Cas9 nuclease (cat. no. 1081058, IDT). CD47-deficient cells were then purified by cell sorting.

Constructs encoding WT mouse (m) CD47, Flag-tagged mCD47 (Flag tag added at the carboxyl terminus), phenylalanine 37-to-aspartate 37 (F37D) mCD47, WT mSLAMF7, arginine 75-to-alanine 75 (R75A) mSLAMF7, glutamate 77-to-alanine 77 (E77A) mSLAMF7, WT mSIRPα, mSIRPα first Ig-like (variable; V) domain, WT hCD47, hSIRPα v.1 (V1) and hSIRPα V2 were generated by PCR or overlap extension PCR. They were then cloned into either the pFB–GFP or the pMIGR–GFP retroviral vector (which used the mouse stem cell virus promoter), which also encode green fluorescent protein (GFP). For L1210 derivatives overexpressing SLAMF7, SLAMF7 was cloned into a promoter-modified pFB–GFP (which used the EF-1α promoter). After transfection in Phoenix-Eco cells, viral supernatants were recovered and used for spin infection of the indicated cell lines or primary cells. Plasmids expressing GFP alone were used as controls. At 48 h after retroviral infection, GFP-positive cells were sorted, expanded and used for experimentation. L1210, EL-4 and BI-141 were sorted twice. L1210 derivatives expressing the Tac antigen were generated as described[5].

Recombinant proteins

To produce Fc fusion proteins containing the extracellular domain of mCD47, mSLAMF7, mSIRPα, mSIRPβ1a, mSIRPβ1b, mSIRPβ1c, hCD47, hSLAMF7, hSLAMF7 first Ig-like (variable; Ig(V)) domain fused to mSLAMF7 second Ig-like (constant; Ig(C)) domain, or mSLAMF7 Ig(V) fused to hSLAMF7 Ig(C), cDNAs were cloned into pFc-hIgG1(LALAPG), which encodes in frame the Fc portion of human IgG1 (hIgG1) with the 'LALAPG' mutations (leucine 234-to-alanine 234; leucine 235-to-alanine 235; proline 329-to-glycine 329) that prevent binding to Fc receptors (FcRs). SIRPα-Fc fusion proteins TTI-621 (ref. 12) and its high-affinity variant ALX148 (ref. 13) were produced by synthesizing the cDNAs from published sequences, followed by cloning into pFc-hIgG1(LALAPG). For production, cDNAs were transfected in 293T cells. Then, fusion proteins were purified with protein A Sepharose (cat. no. GE17-1279-03, Sigma-Aldrich). All recombinant proteins were quantified by SDS–PAGE and Coomassie blue staining, using bovine serum albumin (BSA) as standard.

To produce recombinant versions of soluble mCD47, mSLAMF7, hPD-1 and hPD-L1, cDNAs encoding their extracellular segment, in which a SNAP tag was inserted after the amino-terminal signal peptide and a 10× histidine (His) tag was inserted after the carboxyl terminus of the extracellular domain, were cloned in pPPI4 vector. After transfection in 293T cells, recombinant proteins were purified from cell culture medium using GE Ni Sepharose Excel (GE17371201, Sigma-Aldrich) and eluted with 0.5 M imidazole. Proteins were further purified by size exclusion, using a Superdex 200 Increase 10/300 GL column (cat. no. GE28990944, Sigma-Aldrich), in 4-(2-hydroxyethyl)-1-piperazineethanesulfonic acid (HEPES)-buffered saline buffer (50 mM HEPES-NaOH, pH 7.5, 150 mM NaCl and 10% glycerol). Gel-filtered proteins were labeled either with SNAP-Cell-505 (cat. no. S9103S,

New England Biolabs) or SNAP-Cell-TMR (cat. no. S9105S, New England Biolabs) following the manufacturer's instructions. Free dye was removed using a PD-10 desalting column (cat. no. 87766, Thermo Fisher Scientific). All proteins were quantified by SDS–PAGE and Coomassie blue staining, using BSA as a standard.

Monoclonal antibodies

To generate mSIRPα monoclonal antibodies, *Sirpa*$^{-/-}$ mice were immunized with recombinant mSIRPα-Fc fusion proteins. Splenocytes from hyperimmune mice were then fused with FO cells using polyethylene glycol (cat. no. P7306, Sigma-Aldrich), and cultured in hypoxanthine-aminopterin-thymidine medium for ~8 d. Hybridomas were initially screened by ELISA using the mSIRPα–Fc fusion protein or an irrelevant Fc fusion protein as control. The hybridomas producing mSIRPα antibodies were then subjected to two rounds of sub-cloning. mSIRPα monoclonal antibodies were screened for (1) the capacity to stain EL-4 cells expressing full-length mSIRPα or a variant of mSIRPα containing only the first Ig-like domain, which is implicated in CD47 binding, using flow cytometry; (2) the ability to block the binding of a mCD47-Fc fusion protein to EL-4 cells expressing mSIRPα, using flow cytometry; and (3) the ability to bind SIRPα–Fc, but not SIRPβ-Fc fusion proteins, using ELISA. mSIRPα monoclonal antibodies no. 23 and no. 27 exhibited blocking activity toward SIRPα and did not cross-react with any of the SIRPβ isoforms.

hSLAMF7 hybridomas were generated in a similar way, except that *Slamf7*$^{-/-}$ mice and recombinant hSLAMF7–Fc fusion proteins were utilized. After two rounds of sub-cloning, hSLAMF7 monoclonal antibodies were screened for (1) the ability to bind hSLAMF7–Fc, but not mSLAMF7–Fc. They were then tested for binding to hSLAMF7(V)-mSLAMF7(C)–Fc or mSLAMF7(V)-hSLAMF7(C)–Fc, to determine whether they reacted with the first or second Ig-like domain of hSLAMF7; (2) the capacity to stain EL-4 cells expressing or not hSLAMF7 or *CD47*$^{-/-}$ 293T cells expressing or not hSLAMF7 or the human-mouse SLAMF7 chimeras; and (3) the capacity to block the phagocytosis of *CD47*$^{-/-}$ Raji or *CD47*$^{-/-}$ Daudi by WT BMDMs. hSLAMF7 monoclonal antibodies Z1, Z8, Z9 and Z27 bound specifically to the first Ig-like domain, whereas monoclonal antibodies Z10, Z26, Z30, Z46 and Elo bound specifically to the second Ig-like domain.

Blocking mSLAMF7 monoclonal antibody 4G2 was generated in our laboratory[16]; blocking mCD47 hybridoma Miap301 was provided by T. van den Berg (Sanqin Institute); blocking mSIRPα hybridoma MY-1 was provided by T. Matozaki (Kobe University); and blocking hSLAMF7 hybridoma 162 was reported elsewhere[37].

To create recombinant versions of blocking mSIRPα monoclonal antibody MY-1, blocking mSIRPα monoclonal antibodies no. 23 and no. 27, blocking mCD47 monoclonal antibody Miap301, blocking mSLAMF7 monoclonal antibody 4G2, blocking hSLAMF7 monoclonal antibody 162 and new hSLAMF7 monoclonal antibodies Z1, Z8, Z9, Z10, Z26, Z27, Z30 and Z46, cDNA sequences encoding the variable regions of heavy chain (VH) and light chain (VL) were determined using total cellular RNA from the hybridomas, followed by RNA sequencing or PCR with reverse transcription as described[38]. To create recombinant versions of control IgG monoclonal antibody MOPC21, blocking hSIRPα monoclonal antibodies KWAR23, 18D5, 50A and 40A, blocking hCD47 monoclonal antibodies B6H12 and AO-176, and non-blocking hSLAMF7 monoclonal antibody Elo, VH and VL sequences were obtained from previous studies[14] or patents (WO2017178653A2, US10851164B2, US20200095318, US7709610B2 and EP2569013A2). cDNAs encoding these sequences were then synthesized commercially. In all cases, the VH- and VL-encoding cDNAs were cloned in frame into one or both of the following expression plasmids[38]: pAb-mIgG2a(LALAPG), which contains genes encoding Fc-silent mouse IgG2a (mIgG2a) with the LALAPG mutations, and pAb-mIgK; pAb-hIgG1(LALAPG), which contains genes encoding Fc-silent hIgG1 with the LALAPG mutations and pAb-hIgK. Recombinant monoclonal antibodies were then expressed in 293T cells and purified with protein A Sepharose (cat. no. GE17-1279-03, Sigma-Aldrich). All recombinant monoclonal antibodies were quantified by SDS–PAGE and Coomassie blue staining, using BSA as a standard.

For opsonization of target cells with IgG, Fc-intact Tac monoclonal antibody 7G7 (mIgG2a; BioXCell) and Fc-intact hCD20 monoclonal antibody S18015E (mIgG2a; BioLegend) were used. For flow cytometry assays, we used CD45 monoclonal antibody 30-F11, CD11b monoclonal antibody M1/70, F4/80 monoclonal antibody BM8, Ly6G monoclonal antibody 1A8, NK1.1 monoclonal antibody PK136, SIRPα monoclonal antibody P84, CD64 monoclonal antibody VX54-5/7.1, CD16/32 monoclonal antibody 93, CD18 monoclonal antibody M18/2, CD11a monoclonal antibody M17/4, CD11c monoclonal antibody N418, CD200R1 monoclonal antibody OX-110, Flag monoclonal antibody L5 and anti-rat IgG Poly4054. All were obtained from BioLegend. For immunoprecipitations and immunoblots, we utilized Flag monoclonal antibody M2 (Sigma-Aldrich), Myc monoclonal antibody 9B11 (Cell Signaling Technology), mCD47 monoclonal antibody AF1866 (R&D Systems), anti-mSLAMF7 rabbit antiserum (generated in our laboratory), hCD47 monoclonal antibody D3O7P (Cell Signaling Technology) and hSLAMF7 monoclonal antibody E5C4M (Cell Signaling Technology). β-actin monoclonal antibody AC-74 (Sigma-Aldrich) was used for immunofluorescence.

Phagocytosis assays

Phagocytosis was evaluated using a microscopy-based assay or a pHrodo-based assay, as described[15]. For the microscopy-based assay, 5×10^4 macrophages were seeded in a 24-well tissue culture plate. The next day, target cells were labeled with 2.5 μM of carboxyfluorescein succinimidyl ester (CFSE, cat. no. C34554, Life Technologies). After incubating macrophages in serum-free medium for 1 h, 2×10^5 CFSE-labeled target cells were added to macrophages for 2 h, in the presence or absence of 10 μg ml^{-1} Fc-silent monoclonal antibodies. Macrophages were then washed and imaged with an inverted microscope (Carl Zeiss Axiovert S100 TV). In each experiment, five images per condition were randomly chosen. There were approximately 60–100 macrophages in each image. The phagocytosis efficiency was calculated as the number of macrophages containing CFSE$^+$ target cells per 100 macrophages. For Extended Data Fig. 2c, macrophages or L1210 cells were pre-treated for 30 min with SIRPα monoclonal antibody or CD47 monoclonal antibody, respectively. Cells were then extensively washed to remove unbound antibodies before the phagocytosis assay. For Extended Data Fig. 2h, macrophages were pre-treated with the pro-inflammatory stimulus lipopolysaccharide (cat. no. L4516, Sigma-Aldrich) overnight before the phagocytosis assay. For the pHrodo-based assay, target cells were pre-labeled with 100 ng ml^{-1} of pHrodo green STP ester (cat. no. P35369, Thermo Fisher Scientific), before addition to macrophages. pHrodo dyes are non-fluorescent at neutral pH and become fluorescent in acidic environments such as phagolysosomes. After 2 h, cells were collected and stained with F4/80 monoclonal antibody BM8 (BioLegend) to identify macrophages and analyzed by flow cytometry. For phagocytosis of IgG-opsonized tumor cells, L1210 expressing Tac were opsonized with Tac monoclonal antibody 7G7 (mIgG2a) for 30 min before phagocytosis assays. Raji were opsonized with hCD20 monoclonal antibody S18015E (mIgG2a). For phagocytosis of $C3b_i$-opsonized tumor cells, L1210 was incubated with C5-deficient serum (cat. no. C1163, Sigma-Aldrich) for 30 min, before the phagocytosis assay.

Soluble Fc fusion protein binding assay and flow cytometry

To test binding of the mCD47-Fc fusion protein to cells, BMDMs were detached from plates by treatment with phosphate-buffered saline (PBS) containing 2 mM EDTA and washed. After blocking Fc receptors with a mix of mIgG2a monoclonal antibody 7G7 and CD16/32 monoclonal antibody 2.4G2, cells were incubated for 30 min on

ice with mCD47-Fc (hIgG1) (cat. no. 1866-CD-050, R&D Systems) or mCD47-Fc (hIgG1 LALAPG) (produced in our laboratory). After the incubation period, cells were washed again and incubated for 30 min on ice with Alexa Fluor 647-labeled F(ab′)$_2$ fragments goat anti-human IgG1, Fc-specific (cat. no. 109-606-098, Jackson Immune Research). After additional washes, fluorescence was evaluated by flow cytometry. To examine binding of the mSLAMF7-Fc fusion protein to cells, BI-141 cells expressing or not expressing mSLAMF7 were incubated for 30 min on ice with 10 µg ml^{-1} mCD47 monoclonal antibody (mIgG2a LALAPG). Subsequently, cells were stained with various concentrations of mSLAMF7-Fc (hIgG1 LALAPG) plus Alexa Fluor 647-labeled F(ab′)$_2$ fragments goat anti-human IgG1, Fc-specific (cat. no. 109-606-098, Jackson Immune Research) for 5 min on ice. After additional washes, fluorescence was evaluated by flow cytometry. To determine the impact of SLAMF7 mutations on homotypic binding of SLAMF7, BI-141 cells expressing WT SLAMF7, SLAMF7^{R75A} or SLAMF7^{E77A} were incubated with mSLAMF7-Fc (hIgG1 LALAPG) on ice for 30 min, followed by Alexa Fluor 647-labeled F(ab′)$_2$ fragments goat anti-human IgG1, Fc-specific (cat. no. 109-606-098, Jackson Immune Research) for 30 min on ice before flow cytometry. To ascertain the effect of CD47 mutations on binding to SIRPα, *CD47*$^{-/-}$ 293T cells and *Cd47*$^{-/-}$ L1210 cells expressing WT mCD47 or mutated mCD47^{F37D} were incubated with mSIRPα-Fc (hIgG1 LALAPG) on ice for 30 min. Cells were then washed and incubated with Alexa Fluor 647-labeled Fab′)$_2$ fragments goat anti-human IgG1, Fc-specific (cat. no. 109-606-098, Jackson Immune Research) on ice for 30 min. After additional washes, fluorescence was evaluated by flow cytometry. To detect binding of the hCD47-Fc fusion protein to WT or *CD47*$^{-/-}$ Raji cells, cells were incubated for 30 min on ice with hCD47-Fc (hIgG1 LALAPG). Subsequently, cells were stained with Alexa Fluor 647-labeled F(ab′)$_2$ fragments goat anti-human IgG1, Fc-specific (cat. no. 109-606-098, Jackson Immune Research) for 30 min on ice, followed by flow cytometry. To address the FcR-binding capacity of Fc-silent and Fc-intact monoclonal antibodies, WT BMDMs, which express a wide range of FcRs, were incubated with or without Fc-intact (mIgG2a) or Fc-silent (mIgG2a LALAPG) IgG MOPC21 or Fc-intact (hIgG1) or Fc-silent (hIgG1 LALAPG) hSLAMF7 monoclonal antibody Z10, before flow cytometry. To test whether CD47 or SLAMF7 monoclonal antibodies hindered dye labeling, *CD47*$^{-/-}$ 293T cells, transfected with tagged versions of CD47 or SLAMF7, were stained with Dye 547 or Dye 647 in the presence of control IgG, CD47 monoclonal antibodies or SLAMF7 monoclonal antibodies before the flow cytometry assay. To map the binding site of SLAMF7 monoclonal antibodies on hSLAMF7, *CD47*$^{-/-}$ 293T cells were transfected with the indicated hSLAMF7 plasmids for 48 h, before staining with hSLAMF7 monoclonal antibodies Z10, Z8 or Elo. To determine expression of cell surface markers, Fc receptors were blocked as above, before staining with the indicated antibodies.

Subcutaneous tumor transplantation assay

L1210 (0.5×10^6), L1210 derivatives (0.5×10^6) or Raji (5×10^6) were injected subcutaneously into the right flank of 8–10-week-old *Rag1*$^{-/-}$ or *Rag1*$^{-/-}$*Sirpa*$^{-/-}$ mice. When the tumor was about 5 × 5 mm in diameter, mice were injected intraperitoneally with 200 µg of Fc-silent control IgG monoclonal antibody MOPC21, CD47 monoclonal antibody Miap301, SIRPα monoclonal antibody no. 27, SLAMF7 monoclonal antibody Z10, SLAMF7 monoclonal antibody Elo or CD47 monoclonal antibody B6H12, generated in our laboratory or Fc-intact Tac monoclonal antibody 7G7 and control IgG monoclonal antibody C1.18.4 (BioXCell). Experiments were terminated when or before tumor volume reached 1.5 cm^3. For survival assays, mice were killed when tumors reached 1.5 cm^3. Tumors were then dissected and weighed. Volumes were also assessed. Tumors were sliced into small pieces and digested with 10 µg ml^{-1} deoxyribonuclease I (cat. no. D4513, Sigma-Aldrich) and 25 µg ml^{-1} liberase (cat. no. 5401054001, Sigma-Aldrich). Then, cells were passed through a strainer using the plunger end of a syringe. After washing, total cell numbers were determined. Immune cells were detected by staining with the relevant antibodies and flow cytometry. Macrophages were CD11b$^+$F4/80$^+$; neutrophils were CD11b$^+$Ly6G$^+$; and NK cells were NK1.1$^+$.

Conjugate formation and actin polarization assays

Conjugate formation and actin polarization were tested as described[5]. In brief, for the microscopy-based conjugate formation assay, BMDMs were labeled with CTV and plated overnight. The next day, target cells were labeled with CFSE. Macrophages and target cells were then mixed at a 1:4 ratio in serum-free culture medium in the presence of Fc-silent monoclonal antibodies, and incubated for 20 min at 37 °C to allow conjugate formation. Cells were subsequently washed extensively to remove unconjugated cells. Images were obtained using a LSM710 confocal microscope (Carl Zeiss). Conjugates between BMDMs and target cells were counted. For the flow cytometry-based conjugate formation assay, macrophages were labeled on ice with F4/80 monoclonal antibody BM8 (BioLegend), whereas target cells were labeled with CFSE. After washing, macrophages and targets were mixed with Fc-silent monoclonal antibodies for various periods of time at 37 °C. Conjugates were detected by flow cytometry. To study actin polarization, BMDMs were stained with CTV and seeded onto a confocal tissue dish overnight. The next day, target cells were stained with CFSE. Macrophages and targets were then mixed at a 1:4 ratio in serum-free culture medium with Fc-silent monoclonal antibodies for 20 min at 37 °C. Cells were subsequently fixed, washed and permeabilized and nonspecific staining was blocked in PBS supplemented with 5% BSA for 30 min. Then, cells were washed and incubated for 1 h with β-actin monoclonal antibody AC-74 (Sigma-Aldrich). After washing, cells were incubated for 1 h with Alexa Fluor 647-conjugated anti-mouse IgG (cat. no. 115-605-071, Jackson Immune Research). Cells were then processed and analyzed using a LSM710 confocal microscope (Carl Zeiss). Conjugates with full polarization of actin at the area of contact between the macrophage and the target cell were quantitated.

Immunoprecipitations, immunoblots and mass spectrometry

CD47$^{-/-}$ 293T cells were transiently transfected with plasmids encoding mSLAMF7–Myc, mCD47–Flag or both, or control plasmids, using polyethylenimine (cat. no. 23966, Polysciences). The Myc and Flag tags were located at the carboxyl terminus of the proteins. IP and immunoblot assays were performed as previously described[39]. To test the dissociation of CD47–SLAMF7 interactions by monoclonal antibodies, transfected cells were pre-incubated for 30 min with the indicated monoclonal antibodies. *Cd47*$^{-/-}$ L1210 cells expressing mCD47–Flag and a Brij99-containing lysis buffer were used for mass spectrometry, as reported elsewhere[5]. The following criteria were used to select potentially relevant CD47 interactors (1) presence in Flag immunoprecipitates from *Cd47*$^{-/-}$ L1210 cells expressing CD47-Flag, but not from *Cd47*$^{-/-}$ L1210 cells lacking CD47-Flag; and (2) observation in a minimum of two of three independent experiments.

RNA sequencing

RNA sequencing was performed as described[40]. In essence, RNA was isolated from WT and *Sirpa*$^{-/-}$ BMDMs using the RNeasy Plus Mini kit (cat. no. 74134, QIAGEN), according to the manufacturer's instructions. cDNA libraries were prepared using the Illumina TruSeq Stranded mRNA kit, according to the manufacturer's instructions, and sequenced with the Illumina HiSeq 2000 Sequencer. Read quality was confirmed using FastQC v.0.11.8, before alignment using STAR v.2.5.0 for the mouse GRCm38 v.98 Reference genome. Differential expression analysis was performed with DESeq2 v.1.22.2 from the raw alignment counts calculated with FeatureCounts v.1.5. Differentially expressed genes were defined as genes with an adjusted *P* value of <0.05 and $\log_2$ fold change of ≥1.0.

PLA assay

A PLA was performed with a commercial kit according to the manufacturer's recommendation (cat. no. DUO92008, Duolink In Situ, Sigma-Aldrich). Briefly, after fixing the cells to stabilize proximity, cells were incubated with Fc-silent human IgG1 SLAMF7 monoclonal antibody and Fc-silent mouse IgG2a CD47 monoclonal antibody, followed by oligonucleotide-linked secondary antibodies specifically recognizing each of the primary antibodies. Then, proximity was detected by PCR with complementary oligonucleotides coupled to fluorochromes, and a LSM710 confocal microscope (Carl Zeiss). In each experiment, five images per condition were randomly chosen. A total of 100 cells from three independent experiments were randomly chosen for quantification.

FRET assay

For the FRET assay, constructs encoding SNAP-tagged WT mCD47, mutant mCD47^{F37D} or WT hCD47 were co-transfected with constructs encoding CLIP-tagged WT mSLAMF7, mSLAMF7^{R75A} or mSLAMF7^{E77A} or WT hSLAMF7, into *CD47*$^{-/-}$ 293T cells. After 2 d, cells were collected and seeded onto poly-D-lysine (cat. no. P6407, Sigma-Aldrich)-treated confocal microscopy plates. The next day, cells were labeled with dye SNAP-Surface Alexa Fluor Dye 647 (cat. no. S9136S, New England Biolabs) and dye CLIP-Surface Dye 547 (cat. no. S9233S, New England Biolabs) for 45 min at 37 °C, in the presence of 10 µg ml^{-1} of Fc-silent monoclonal antibodies. Cells were then fixed with 4% paraformaldehyde (cat. no. 22023, Biotium) and washed, before the FRET assay. Images were acquired with an LSM710 confocal microscope (Carl Zeiss) by exciting Dye 547 (energy donor) at 543 nm and Dye 647 (energy acceptor) at 635 nm. Images before and after acceptor bleaching were acquired for FRET efficiency analysis, using ImageJ (Fiji) with the AccPbFRET plugin, as previously described[30,41].

LUV reconstitution assay

LUVs reconstitution followed by FRET assay was performed as described[29]. For LUV preparation, 80% 1-palmitoyl-2-oleoyl-glycero-3-phosphocholine (cat. no. 850457C, Avanti Polar Lipids) and 20% 1,2-dioleoyl-sn-glycero-3-((N-(5-amino-1-carboxypentyl)iminodiacetic acid)succinyl) (nickel salt) (DGS-NTA-Ni, cat. no. 790404C, Avanti Polar Lipids) were mixed in chloroform, dried under a stream of nitrogen, desiccated for 1 h in a vacuum container and then resuspended in PBS. LUVs were generated by extrusion 20 times through a pair of polycarbonate filters containing pores of 200 nm diameter. 8.3 nM SNAP-Cell-505-labeled mSLAMF7-His or hPD-L1-His was mixed with 0.23 nM LUVs harboring DGS-NTA-Ni in PBS containing 1.5 mg ml^{-1} BSA and 1 mM tris(2-carboxyethyl)phosphine in a 96-well solid black microplate, during which the SNAP-Cell-505 fluorescence was monitored in real time, using a plate reader with 504-nm excitation and 540-nm emission. After 30 min, the fluorescence reading was paused and the second protein component (25 nM SNAP-Cell-TMR-labeled mCD47-His or hPD-1-His), was injected and the fluorescence was monitored for another 30 min. For some conditions, SNAP-Cell-505-labeled mCD47-His or SNAP-Cell-TMR-labeled mSLAMF7-His was incubated with Fc-silent monoclonal antibodies (threefold molar excess) for 30 min before being added to the reaction. Data were normalized for the MFI of the last ten data points, before the addition of SNAP-Cell-TMR-labeled protein and plotted with GraphPad Prism.

Statistical analyses

Prism v.9 software (GraphPad) was used for paired or unpaired Student's *t*-tests (two-tailed) and for one-way analysis of variance followed by Tukey's or Dunnett's multiple comparison tests, when appropriate. The normal distribution of the data was tested using the D'Agostino-Pearson normality test (Prism v.9) and parametric tests used for statistical analyses accordingly.

Sample size, statistical tests, randomization and blinding

Sample size was chosen based on our previous studies with the experimental protocols used, to ensure adequate reproducibility[15]. Age- and sex-matched mice were used for all experiments. Experimental allocations were random. Investigators were not blinded to genotypes before data collection. Blinding was not relevant to the study because all analyses were strictly quantitative and non-subjective measures were used to understand the phenotypes observed. All the findings were based on two, three or more independent experiments and were reproducible. No data were excluded from the analyses.

Reporting summary

Further information on research design is available in the Nature Portfolio Reporting Summary linked to this article.

Data availability

RNA-seq data supporting the findings of this study have been deposited into the Gene Expression Omnibus under accession no. GSE223059. All other relevant data are available from the corresponding author upon reasonable request. Source data are provided with this paper.

References

35. Guo, H. et al. Deletion of Slam locus in mice reveals inhibitory role of SLAM family in NK cell responses regulated by cytokines and LFA-1. *J. Exp. Med.* **213**, 2187–2207 (2016).
36. Abraham, N., Miceli, M. C., Parnes, J. R. & Veillette, A. Enhancement of T-cell responsiveness by the lymphocyte-specific tyrosine protein kinase p56lck. *Nature* **350**, 62–66 (1991).
37. Bouchon, A., Cella, M., Grierson, H. L., Cohen, J. I. & Colonna, M. Activation of NK cell-mediated cytotoxicity by a SAP-independent receptor of the CD2 family. *J. Immunol.* **167**, 5517–5521 (2001).
38. von Boehmer, L. et al. Sequencing and cloning of antigen-specific antibodies from mouse memory B cells. *Nat. Protoc.* **11**, 1908–1923 (2016).
39. Davidson, D. et al. The Csk-associated adaptor PAG inhibits effector T cell activation in cooperation with phosphatase PTPN22 and Dok adaptors. *Cell Rep.* **17**, 2776–2788 (2016).
40. Zhong, M. C. et al. SLAM family receptors control pro-survival effectors in germinal center B cells to promote humoral immunity. *J. Exp. Med.* **218**, e20200756 (2021).
41. Roszik, J., Szollosi, J. & Vereb, G. AccPbFRET: an ImageJ plugin for semi-automatic, fully corrected analysis of acceptor photobleaching FRET images. *BMC Bioinform.* **9**, 346 (2008).

Acknowledgements

We thank members of the Veillette laboratory for useful discussions. We also acknowledge T. van den Berg (Amsterdam) and T. Matozaki (Kobe) for providing hybridomas. This work was supported by grants from the Canadian Institutes of Health Research (MT-14429, MOP-82906, FDN-143338, PJT-178314 and PJT-183593), the Terry Fox Research Institute (1190-02) and the Ministère de l'économie et de l'innovation (Québec) to A.V.; and US National Institutes of Health grant R37 CA239072 to E.H. A.V. received a contract from Bristol Myers-Squibb to study the mechanism of action of SLAMF7 monoclonal antibody elotuzumab against multiple myeloma. Z.T. received a Fellowship from the Cole Foundation; C.C.G. received a Studentship from the Fonds de la recherche en santé – Québec; J.L. receives a Studentship from the Chinese Science Council; and A.V. holds the Canada Research Chair on Signaling in the Immune System.

Author contributions

Z.T., M.C.-Z., J.Q., D.D., Y.Z., E.H. and A.V. designed experiments. Z.T., M.C.-Z., J.Q., C.C.G., J.L. and Y.Z. performed experiments. All authors interpreted the results. Z.T. and A.V. wrote the manuscript. All authors commented on the manuscript. A.V. and E.H. provided funding.

Competing interests

Members of the Veillette laboratory will file a patent on the use of monoclonal antibody Z10 for the treatment of SLAMF7-positive human tumors. The authors declare no other competing interests.

Additional information

Extended data is available for this paper at https://doi.org/10.1038/s41590-023-01671-2.

Supplementary information The online version contains supplementary material available at https://doi.org/10.1038/s41590-023-01671-2.

Correspondence and requests for materials should be addressed to André Veillette.

Peer review information *Nature Immunology* thanks David Raulet and the other, anonymous, reviewer(s) for their contribution to the peer review of this work. Primary Handling Editor: Ioana Visan, in collaboration with the *Nature Immunology* team. Peer reviewer reports are available.

https://doi.org/10.1038/s41590-023-01671-2

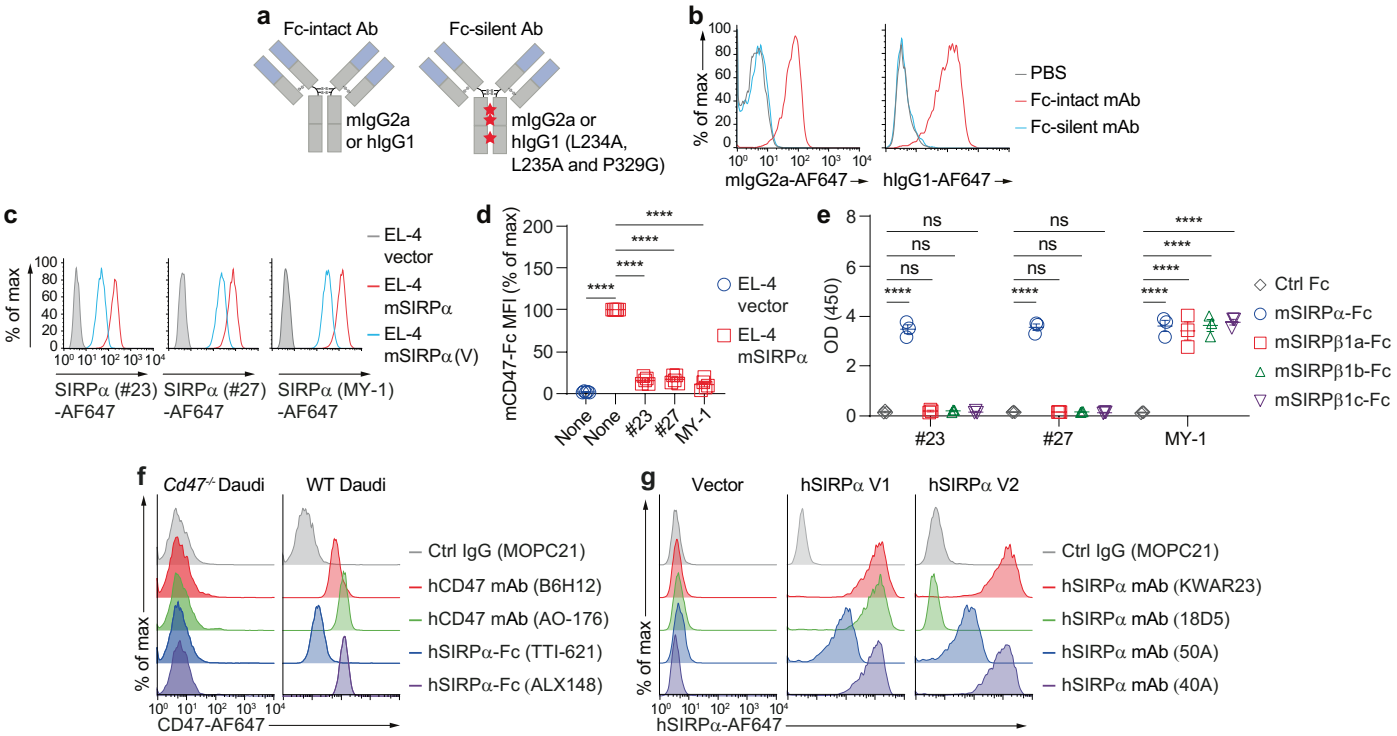

Extended Data Fig. 1 | Generation of Fc-silent mAbs. a, The three mutations ('LALAPG') introduced in the Fc portion of mAbs to render them Fc-silent are depicted. LALAPG is L234A ('LA'), L235A ('LA'), and P329G ('PG'). **b**, Binding assay of Fc-intact and Fc-silent variants of mIgG2a (mAb MOPC21) or hIgG1 (mAb Z10) to FcRs on BMDMs assessed by flow cytometry. **c**, Binding of Fc-silent mSIRPα mAbs #23, #27 and MY-1 to EL-4 cells and EL-4 cells expressing full-length mSIRPα or a variant of mSIRPα containing only the first Ig-like variable (V) domain assessed by flow cytometry. **d**, Binding of a soluble mCD47-Fc fusion protein to EL-4 cells, expressing or not expressing mSIRPα, studied by flow cytometry. MFI, mean fluorescence intensity. **e**, Binding of Fc-silent mSIRPα mAbs #23, #27 and MY-1 to mSIRPα-Fc, mSIRPβ1a-Fc, mSIRPβ1b-Fc and mSIRPβ1c-Fc, determined by ELISA. **f**, Binding of Fc-silent Ctrl IgG MOPC21, hCD47 mAbs B6H12 and AO-176 or hSIRPα-Fc fusion proteins TTI-621 and ALX148 to WT and *CD47*$^{-/-}$ Daudi cells evaluated by flow cytometry. **g**, Binding of Fc-silent hSIRPα mAbs to *Sirpa*$^{-/-}$ BMDMs, transduced with retroviruses encoding or not encoding the V1 or V2 version of hSIRPα, studied by flow cytometry. All data are means ± s.e.m. ****$p < 0.0001$. Flow cytometry profiles are representative of 3 (**c**,**f**,**g**) or 2 (**b**) independent experiments. Results are pooled from 5 (**d**) and 3 (**e**) independent experiments.

https://doi.org/10.1038/s41590-023-01671-2

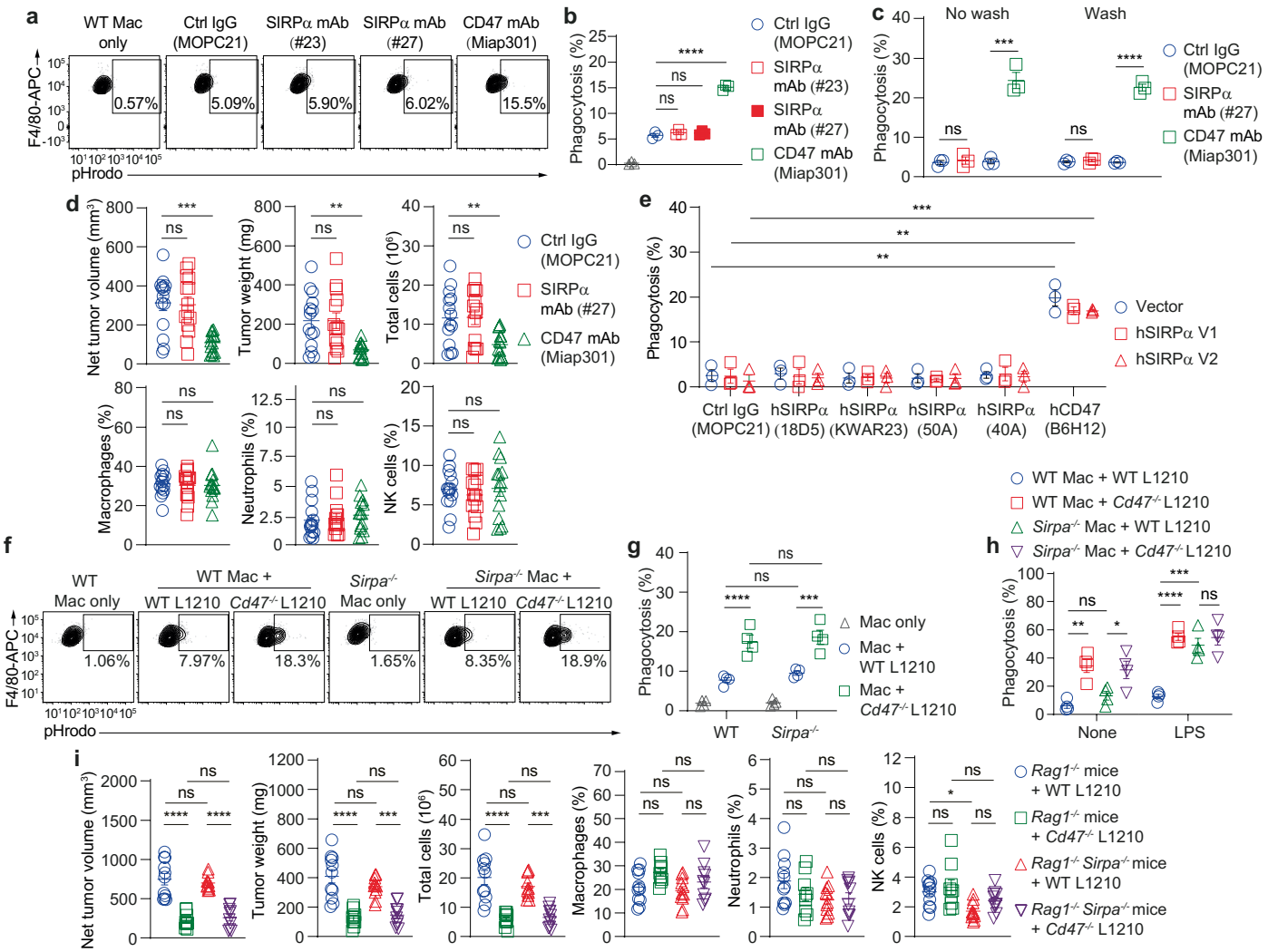

Extended Data Fig. 2 | CD47, but not SIRPα, inhibits SLAMF7-mediated phagocytosis. a,**b**, Representative flow cytometry profiles (a) and compiled data from 3 independent experiments (b) of phagocytosis assays of L1210 cells by WT BMDMs, assessed by flow cytometry using the pHrodo dye as in Fig. 1b. **c**, Phagocytosis assays of L1210 cells by WT BMDMs as in Fig. 1b. BMDMs and L1210 cells were pre-treated with indicated mAbs, followed or not by extensive washing, prior to the phagocytosis assay. **d**, Tumors from the experiment depicted in Fig. 1e were dissected, weighed, measured, and analyzed by flow cytometry. **e**, Phagocytosis of Raji cells by *Sirpa*$^{-/-}$ BMDMs, expressing or not expressing hSIRP*α* version V1 or V2 as in Fig. 1f. **f**,**g**, Representative flow cytometry profiles (f) and compiled data from 4 independent experiments (g) of phagocytosis assays of WT and *Cd47*$^{-/-}$ L1210 cells by WT or *Sirpa*$^{-/-}$ BMDMs, assessed by flow cytometry using the pHrodo dye as in Fig. 2a. **h**, Phagocytosis assays of WT and *Cd47*$^{-/-}$ L1210 cells by WT or *Sirpa*$^{-/-}$ BMDMs, with or without pre-treatment of lipopolysaccharide (LPS), as in Fig. 2a. **i**, Tumors from the experiment depicted in Fig. 2e were dissected, weighed, measured and analyzed by flow cytometry. One mouse from '*Rag1*$^{-/-}$ mice + *Cd47*$^{-/-}$ L1210' group showed no clinically detectable tumor on day 17. All data are means ± s.e.m. ns, not significant; *p < 0.05, **p < 0.01, ***p < 0.001, and ****p < 0.0001. Flow cytometry profiles are representative of 3 (**a**) or 4 (**f**) independent experiments. Results are pooled from 3 (**b**,**c**,**e**) or 4 (**g**,**h**) mice studied in 3 (**b**,**c**,**e**) or 4 (**g**,**h**) independent experiments, 14 (**d**) mice from 3 independent experiments, and 11 (WT L1210) or 10 (*Cd47*$^{-/-}$ L1210) mice from 2 independent experiments (**i**). Each symbol represents one mouse.

https://doi.org/10.1038/s41590-023-01671-2

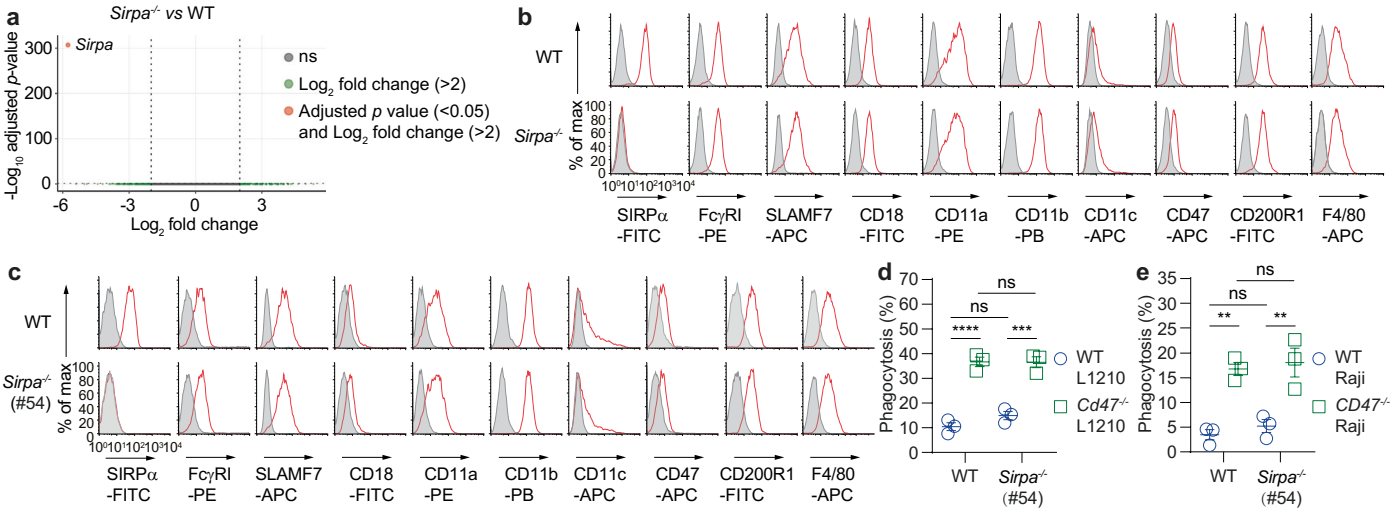

Extended Data Fig. 3 | Loss of SIRPa does not alter macrophage differentiation. a, RNA sequence of *Sirpa*$^{-/-}$ vs WT BMDMs was analyzed. **b**, expression of various cell surface markers (red lines) in WT and *Sirpa*$^{-/-}$ BMDMs assayed by flow cytometry. Filled curves, Ctrl IgG. **c**, expression of various cell surface markers (red lines) in WT and *Sirpa*$^{-/-}$ BMDMs from a second *Sirpa*$^{-/-}$ C57BL/6 mouse strain (#54) assayed by flow cytometry. Filled curves, Ctrl IgG. **d**,**e**, Phagocytosis of L1210 cells (**d**) and Raji cells (**e**), expressing or not expressing CD47, by WT or *Sirpa*$^{-/-}$ BMDMs as in Fig. 2a. All data are means ± s.e.m. ns, not significant; **p < 0.01, ***p < *0.001*, and ****p < 0.0001. 3 pairs of mice were studied in one experiment (**a**). Flow cytometry profiles are representative of 3 (**b**,**c**) independent experiments. Results are pooled from a total of 3 (**d**,**e**) mice studied in 3 independent experiments. Each symbol represents one mouse.

https://doi.org/10.1038/s41590-023-01671-2

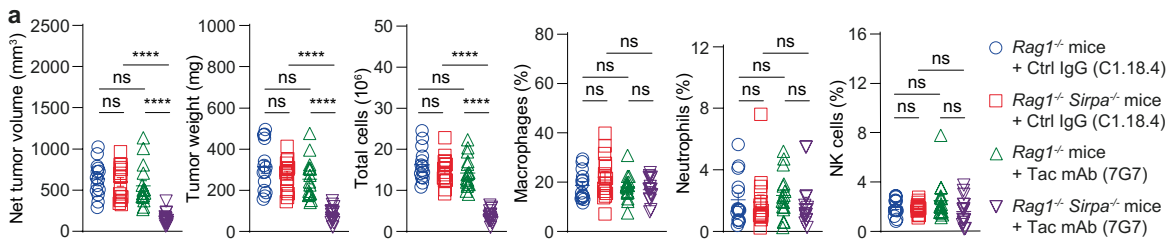

Extended Data Fig. 4 | Both CD47 and SIRPα inhibit FcR-mediated tumor growth. Tumors from the experiment depicted in Fig. 3d were dissected, weighed, measured and analysed by flow cytometry. One mouse from '*Rag1*$^{-/-}$ mice + Ctrl IgG (C1.18.4)' group showed no clinically detectable tumor on day 18. All data are means ± s.e.m. ns, not significant; ****p < 0.0001. Results are pooled from a total of 15 mice [16 mice for '*Rag1*$^{-/-}$ mice + Tac mAb (7G7)' group] from 3 independent experiments. Each symbol represents one mouse.

https://doi.org/10.1038/s41590-023-01671-2

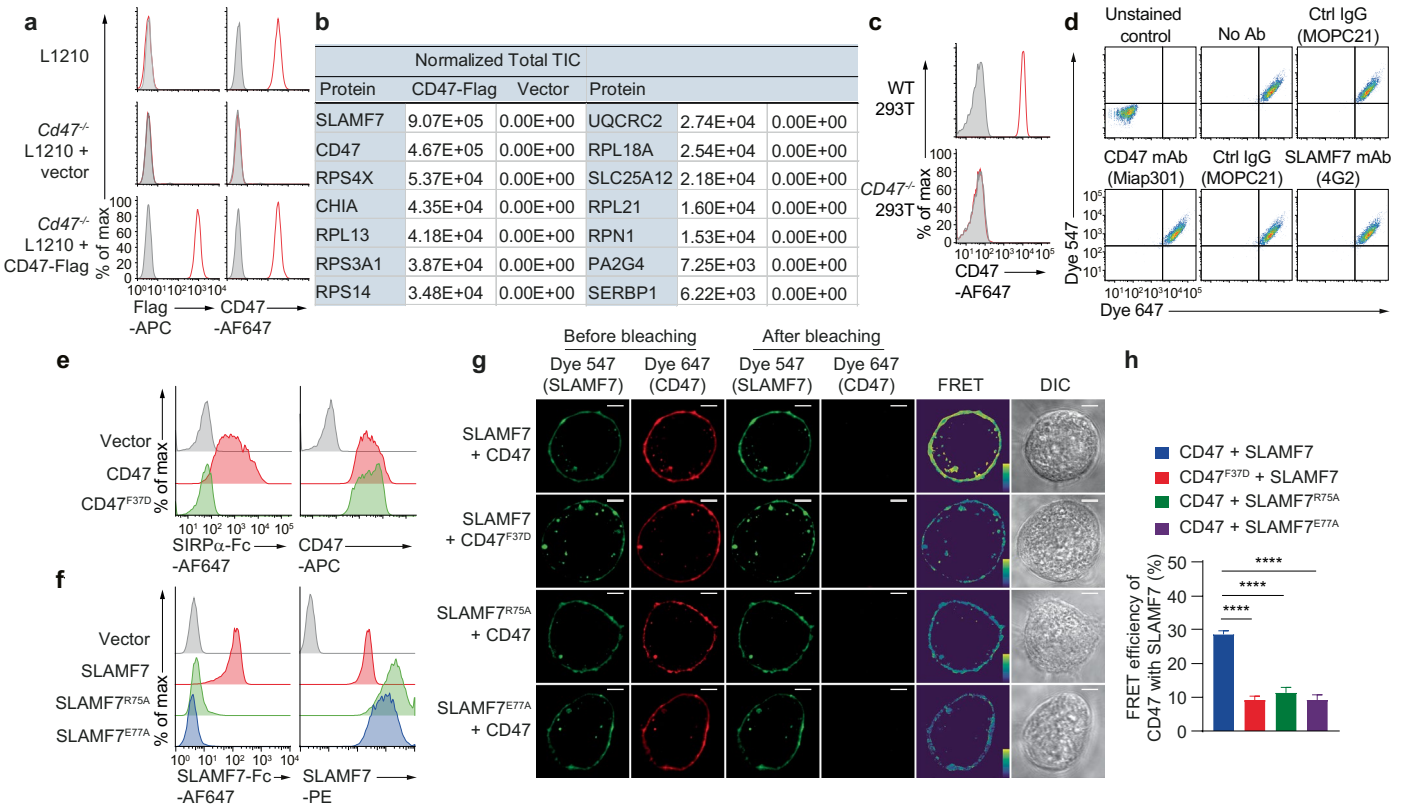

Extended Data Fig. 5 | CD47 interacts in *cis* with SLAMF7. a, Expression of Flag or CD47 (red lines) on L1210 cells and *Cd47*$^{-/-}$ L1210 cells, expressing or not expressing mCD47-Flag, assessed by flow cytometry. Permeabilization was used for the Flag staining. Filled curves, Ctrl IgG. **b**, Means of the normalized total ion current (TIC) for the potential interactors of CD47. **c**, Expression of hCD47 (red lines) on WT or *CD47*$^{-/-}$ 293 T cells was assessed by flow cytometry. Filled curves, Ctrl IgG. **d**, Fluorescence intensity of Dye 647 and Dye 547 in *CD47*$^{-/-}$ 293 T cells, transfected with tagged versions of mCD47 and mSLAMF7 and treated with or without Ctrl IgG, mCD47 mAb and mSLAMF7 mAb, assayed by flow cytometry. **e**, Binding of soluble mSIRPα-Fc fusion protein and expression of mCD47 on transfected *CD47*$^{-/-}$ 293 T cells assessed by flow cytometry. **f**, Binding of soluble mSLAMF7-Fc fusion protein and expression of mSLAMF7 on transfected BI-141 cells assessed by flow cytometry. **g**,**h**, Representative confocal microscopy images (**g**) and compiled data from 18 cells in 3 independent experiments (**h**) of FRET assays as in Fig. 4d,e. All data are means ± s.e.m. ns, not significant; ****$p < 0.0001$. Flow cytometry profiles are representative of 3 (**a**,**c**-**f**) independent experiments. Results are representative of 3 (**g**) independent experiments. Results are pooled from 3 (**b**,**h**) independent experiments.

https://doi.org/10.1038/s41590-023-01671-2

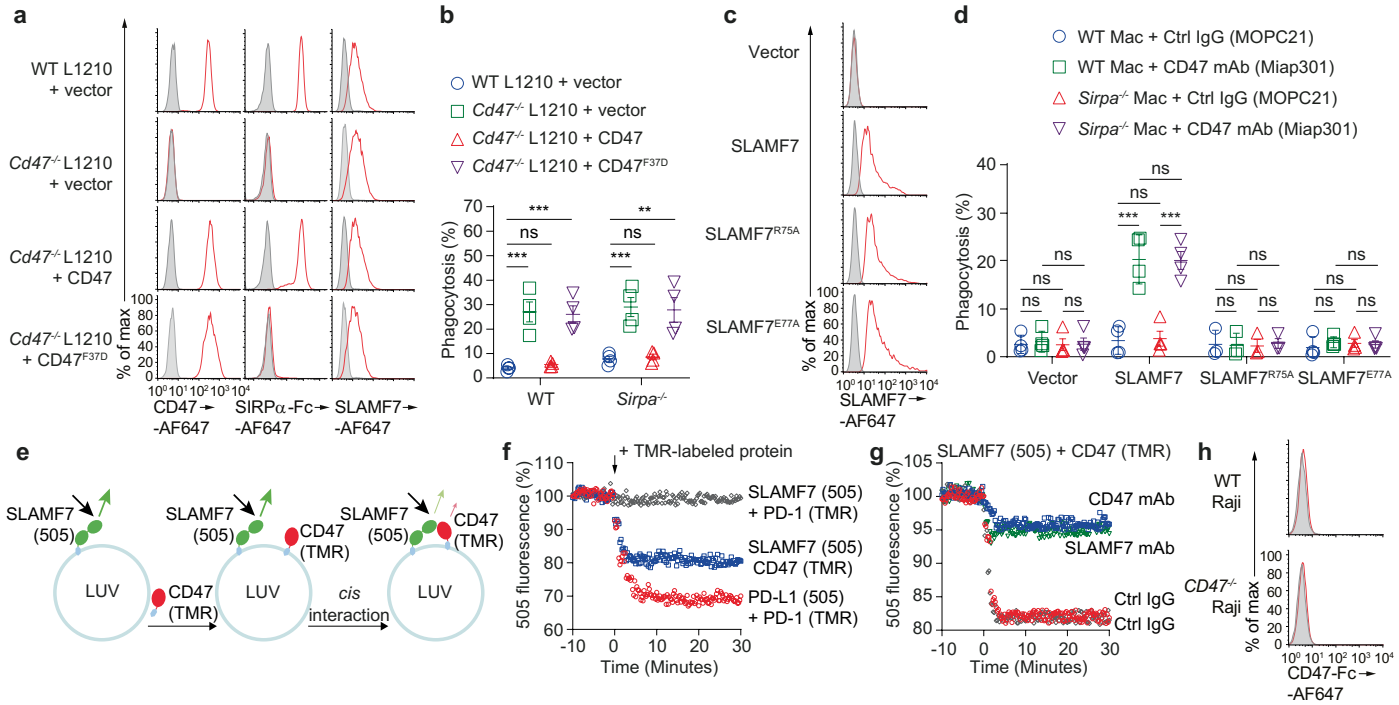

Extended Data Fig. 6 | Structure-function analyses of CD47 and SLAMF7. **a**, Expression of mCD47 and mSLAMF7 and binding of mSIRPα-Fc (red lines) in L1210 derivatives assessed by flow cytometry. Filled curves, Ctrl IgG or Ctrl Fc fusion protein. **b**, Phagocytosis assays of L1210 derivatives by WT or *Sirpa*$^{-/-}$ BMDMs as in Fig. 2a. **c**, Expression of mSLAMF7 (red lines) in *Slamf7*$^{-/-}$ conA-activated CD4^{+} T cells, transduced with variants of mSLAMF7 constructs, assessed by flow cytometry. Filled curves, Ctrl IgG. **d**, Phagocytosis assays of conA-activated CD4^{+} T cells by WT or *Sirpa*$^{-/-}$ BMDMs as in Fig. 2a. **e**,**f**, Schematic representation (e) and time-course of normalized dye 505 fluorescence intensity (f) of LUV-based FRET assay of mSLAMF7 (donor) or hPD-L1 (donor) with mCD47 (acceptor) or hPD-1 (acceptor) monitored by a real time plate reader. **g**, Time-course of normalized dye 505 fluorescence intensity of LUV-based FRET assay of mSLAMF7 (donor) with mCD47 (acceptor), pre-treated with Ctrl IgG MOPC21, mSLAMF7 mAb 4G2 and mCD47 mAb Miap301, monitored by a real time plate reader. **h**, Binding of soluble hCD47-Fc fusion protein to WT or *CD47*$^{-/-}$ Raji cells assessed by flow cytometry. All data are means ± s.e.m. ns, not significant; $^{**}p < 0.01$ and $^{***}p < 0.001$. Flow cytometry profiles are representative of 3 (**a**,**c**) or 2 (**h**) independent experiments. Results are representative of 3 (**f**) or 2 (**g**) independent experiments. Results are pooled from 4 (**b**) or 4 (**d**; for all variants, except 3 for SLAMF7^{R75A}) independent experiments. Each symbol represents one mouse.

https://doi.org/10.1038/s41590-023-01671-2

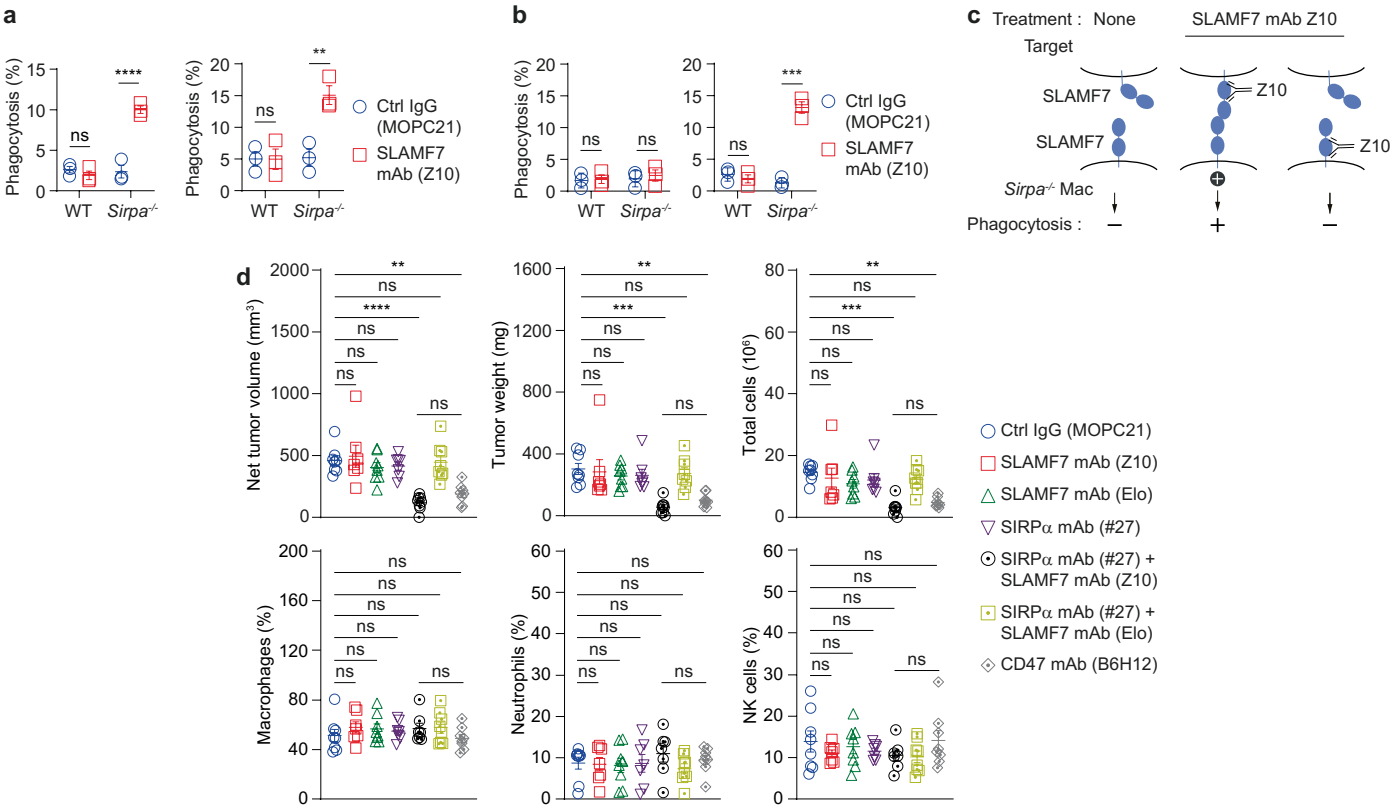

Extended Data Fig. 7 | mAb Z10 promotes phagocytosis with SIRPα blockade. **a**,**b**, Phagocytosis assay of Daudi (a, left), MM.1 S (a, right), and Fc-silent CD3 + CD28 mAbs activated mouse $CD8^+$ T cells expressing (b, right) or not expressing (b, left) hSLAMF7 by WT or *Sirpa*$^{-/-}$ BMDMs assayed by fluorescence microscopy. **c**, Schematic representations of the impact of mAb Z10 on macrophages or target cells. **d**, Tumors from experiment depicted in Fig. 6g were dissected, weighed, measured, and analysed by flow cytometry. One mouse showed no detectable tumor in the 'SIRPα mAb (#27) + SLAMF7 mAb (Z10)' group on day 24. All data are means ± s.e.m. ns, not significant; $^{**}p < 0.01$, $^{***}p < 0.001$, and $^{****}p < 0.0001$. Results are pooled from 3 (**a**,**b**) mice studied in 3 (**a**,**b**) independent experiments; 8 [except 7 for 'SLAMF7 mAb (Z10)' and 'SIRPα mAb (#27)' groups] mice from 2 independent experiments (**d**). Each symbol represents one mouse.

https://doi.org/10.1038/s41590-023-01671-2

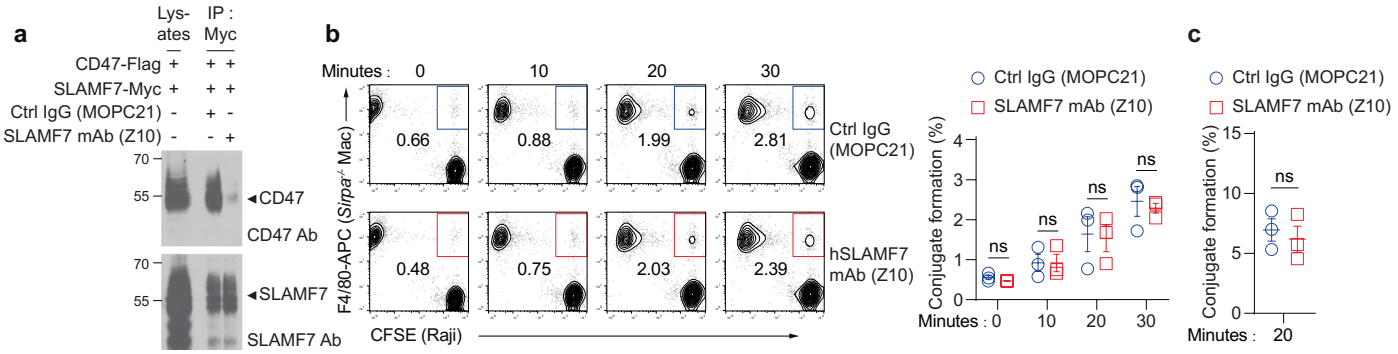

Extended Data Fig. 8 | Z10 disrupts CD47-SLAMF7 interaction and does not affect conjugate formation. a, Co-immunoprecipitation assay of CD47 and SLAMF7 in *CD47*$^{-/-}$ 293 T cells expressing a Flag-tagged variant of hCD47 and a Myc-tagged variant of hSLAMF7, in the presence of Ctrl IgG MOPC21 or hSLAMF7 mAb Z10. **b**, Representative flow cytometry profiles (b, left) and compiled data from 3 independent experiments (b, right) of conjugate formation assays of *Sirpa*$^{-/-}$ BMDMs with Raji cells for the indicated time points, in the presence of Ctrl IgG or hSLAMF7 mAb Z10, detected by flow cytometry. **c**, Conjugate formation assays of *Sirpa*$^{-/-}$ BMDMs with Raji cells for 20 minutes, assessed by confocal microscopy. All data are means ± s.e.m. ns, not significant. Results are representative of 2 (**a**) independent experiments. Flow cytometry profiles are representative of 3 independent experiments (**b**). Results are pooled from a total of 3 (**b**,**c**) mice studied in 3 (**b**,**c**) independent experiments. Each symbol represents one mouse.

https://doi.org/10.1038/s41590-023-01671-2

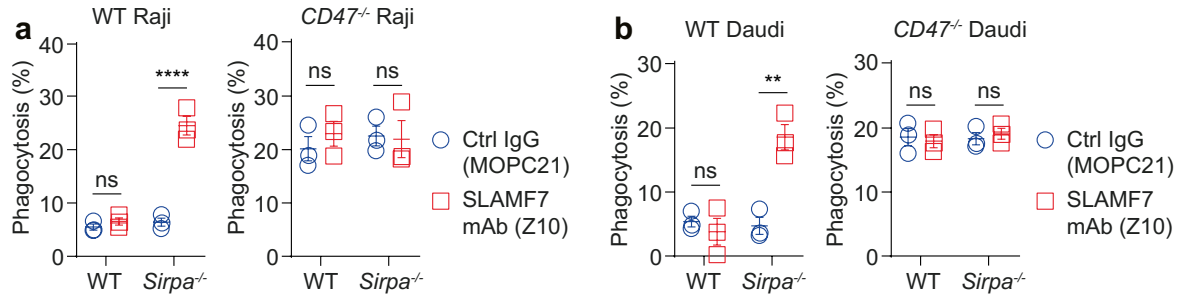

Extended Data Fig. 9 | Z10 does not interfere with phagocytosis of CD47-deficient targets. a,**b**, Phagocytosis of Raji (a) and Daudi (b), expressing or not expressing CD47 by WT or *Sirpa*$^{-/-}$ BMDMs in the presence of Ctrl IgG MOPC21 and hSLAMF7 mAb Z10 assayed by fluorescence microscopy. All data are means ± s.e.m. ns, not significant; $^{**}p < 0.01$ and $^{****}p < 0.0001$. Results are pooled from 3 (**a**,**b**) mice studied in 3 independent experiments. Each symbol represents one mouse.

https://doi.org/10.1038/s41590-023-01671-2

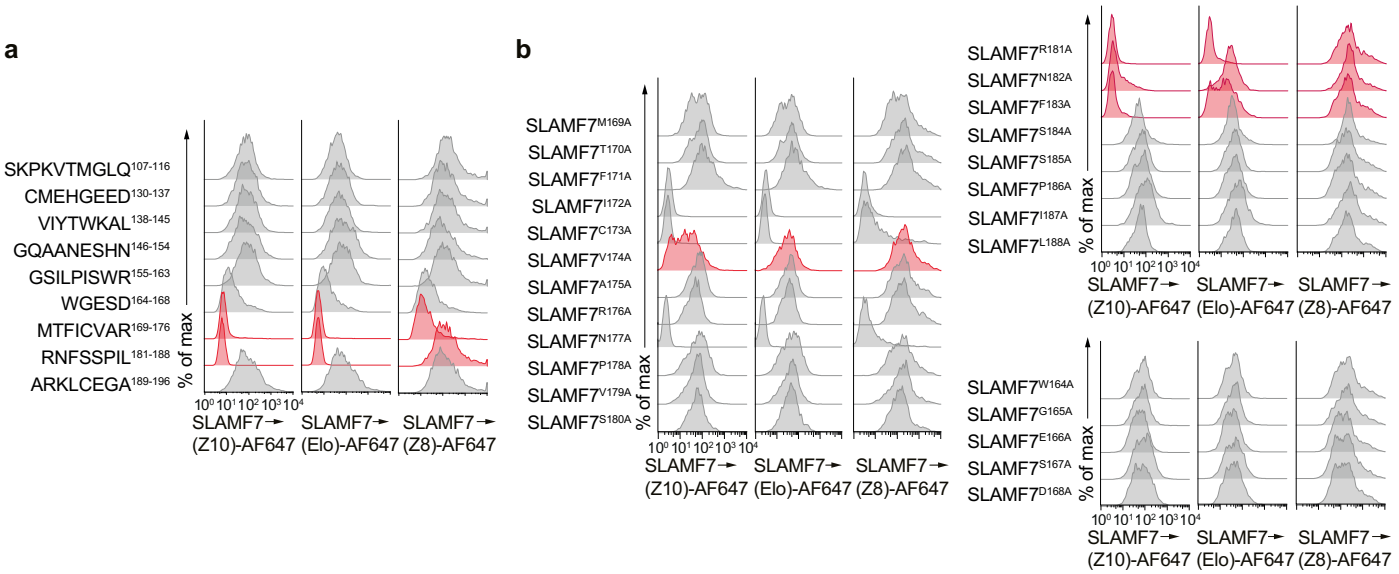

Extended Data Fig. 10 | Z10 binds to the second Ig-like domain of SLAMF7. **a**,**b**, Binding of hSLAMF7 mAbs Z10, Elo and Z8 to *CD47*$^{-/-}$ 293 T cells expressing various chimeras between hSLAMF7 and mSLAMF7 (a) or various mutants of hSLAMF7 (b), assayed by flow cytometry. For the chimeras, the residues in hSLAMF7 (numbered) were replaced by the equivalent residues in mSLAMF7. Flow cytometry profiles are representative of 3 (**a**,**b**, except 2 for hSLAMF7^{N177A}, hSLAMF7^{P178A}, hSLAMF7^{V179A}, hSLAMF7^{S180A}) independent experiments.

nature portfolio

Corresponding author(s): André Veillette

Last updated by author(s): Sep 29, 2023

Reporting Summary

Nature Portfolio wishes to improve the reproducibility of the work that we publish. This form provides structure for consistency and transparency in reporting. For further information on Nature Portfolio policies, see our Editorial Policies and the Editorial Policy Checklist.

Statistics

For all statistical analyses, confirm that the following items are present in the figure legend, table legend, main text, or Methods section.

n/a	Confirmed	
☐	☒	The exact sample size (*n*) for each experimental group/condition, given as a discrete number and unit of measurement
☐	☒	A statement on whether measurements were taken from distinct samples or whether the same sample was measured repeatedly
☐	☒	The statistical test(s) used AND whether they are one- or two-sided *Only common tests should be described solely by name; describe more complex techniques in the Methods section.*
☒	☐	A description of all covariates tested
☐	☒	A description of any assumptions or corrections, such as tests of normality and adjustment for multiple comparisons
☐	☒	A full description of the statistical parameters including central tendency (e.g. means) or other basic estimates (e.g. regression coefficient) AND variation (e.g. standard deviation) or associated estimates of uncertainty (e.g. confidence intervals)
☐	☒	For null hypothesis testing, the test statistic (e.g. *F*, *t*, *r*) with confidence intervals, effect sizes, degrees of freedom and *P* value noted *Give P values as exact values whenever suitable.*
☒	☐	For Bayesian analysis, information on the choice of priors and Markov chain Monte Carlo settings
☒	☐	For hierarchical and complex designs, identification of the appropriate level for tests and full reporting of outcomes
☒	☐	Estimates of effect sizes (e.g. Cohen's *d*, Pearson's *r*), indicating how they were calculated

Our web collection on statistics for biologists contains articles on many of the points above.

Software and code

Policy information about availability of computer code

Data collection	Carl Zeiss Axiovert S100 microscope and Carl Zeiss LSM710 confocal microscope were used for capturing images. CyAn ADP analyzer and BD LSR Fortessa were used for flow cytometry.
Data analysis	FlowJo V10.6.2 was used to analyze flow cytometry data. Prism v9 was used for statistical analyses. SnapGene Viewer 4.2.6 was used to analyze DNA sequencing data. FastQC v0.10.1, TopHat v2.0.10, DESeq2 v1.14.1 and FeatureCounts v1.4.6 were used to analyze RNA-Seq data.

For manuscripts utilizing custom algorithms or software that are central to the research but not yet described in published literature, software must be made available to editors and reviewers. We strongly encourage code deposition in a community repository (e.g. GitHub). See the Nature Portfolio guidelines for submitting code & software for further information.

Data

Policy information about availability of data

All manuscripts must include a data availability statement. This statement should provide the following information, where applicable:

- Accession codes, unique identifiers, or web links for publicly available datasets
- A description of any restrictions on data availability
- For clinical datasets or third party data, please ensure that the statement adheres to our policy

RNA-Seq data supporting the findings of this study have been deposited into the Gene Expression Omnibus (GEO) database under accession number GSE223059.

Human research participants

Policy information about studies involving human research participants and Sex and Gender in Research.

Reporting on sex and gender	Blood from both sexes was randomly used in this study.
Population characteristics	Only 4 healthy human participants donated blood, so no covariate-relevant population characteristics can be determined.
Recruitment	A poster outlining the following requirements were published within the IRCM building: Men and women; Over 18 years old; In good health; Without known acute or chronic disease. Interested participants then contacted nurse through the IRCM clinic for consent form signature and blood drawing. Blood samples were then labeled by a project number and handed over for analyses to researchers. Given that IRCM internal community has no restriction to any particular demographic group (sex, age, ethnicity, etc.), it is unlikely that biases were introduced at the recruitment stage.
Ethics oversight	Collection of human blood samples was approved by the IRCM Human Ethics Board, and informed consent form was signed by the participants prior to taking a sample of blood.

Note that full information on the approval of the study protocol must also be provided in the manuscript.

Field-specific reporting

Please select the one below that is the best fit for your research. If you are not sure, read the appropriate sections before making your selection.

☒ Life sciences ☐ Behavioural & social sciences ☐ Ecological, evolutionary & environmental sciences

For a reference copy of the document with all sections, see nature.com/documents/nr-reporting-summary-flat.pdf

Life sciences study design

All studies must disclose on these points even when the disclosure is negative.

Sample size	Sample size was chosen based on our previous studies with the experimental protocols to ensure adequate reproducibility. (https://doi.org/10.1038/nature22076, https://doi.org/10.1016/j.celrep.2021.110111)
Data exclusions	No data were excluded from the analyses.
Replication	All findings were based on 2, 3 or more independent experiments and were reproducible.
Randomization	Experimental allocations were random. Age- and sex-matched mice were used for experiments.
Blinding	Investigators were not blinded to genotypes prior to data collection. Blinding was not relevant to the study because all analyses were strictly quantitative and non-subjective measures were used to understand the phenotypes observed.

Behavioural & social sciences study design

All studies must disclose on these points even when the disclosure is negative.

Study description	Not applicable
Research sample	Not applicable
Sampling strategy	Not applicable
Data collection	Not applicable
Timing	Not applicable
Data exclusions	Not applicable
Non-participation	Not applicable
Randomization	Not applicable

Ecological, evolutionary & environmental sciences study design

All studies must disclose on these points even when the disclosure is negative.

Study description	Not applicable
Research sample	Not applicable
Sampling strategy	Not applicable
Data collection	Not applicable
Timing and spatial scale	Not applicable
Data exclusions	Not applicable
Reproducibility	Not applicable
Randomization	Not applicable
Blinding	Not applicable

Did the study involve field work? ☐ Yes ☒ No

Reporting for specific materials, systems and methods

We require information from authors about some types of materials, experimental systems and methods used in many studies. Here, indicate whether each material, system or method listed is relevant to your study. If you are not sure if a list item applies to your research, read the appropriate section before selecting a response.

Materials & experimental systems

n/a	Involved in the study
☐	☒ Antibodies
☐	☒ Eukaryotic cell lines
☒	☐ Palaeontology and archaeology
☐	☒ Animals and other organisms
☒	☐ Clinical data
☒	☐ Dual use research of concern

Methods

n/a	Involved in the study
☒	☐ ChIP-seq
☐	☒ Flow cytometry
☒	☐ MRI-based neuroimaging

Antibodies

Antibodies used

Anti-mouse CD11b pacific blue, (M1/70) Biolegend Cat# 101224; RRID:AB_755986 Validation https://www.biolegend.com/en-us/products/pacific-blue-anti-mouse-human-cd11b-antibody-3863 Dilution 1:100
Anti-mouse CD18 FITC, (M18/2) Biolegend Cat# 101405; RRID:AB_312814 Validation https://www.biolegend.com/en-us/products/fitc-anti-mouse-cd18-antibody-358 Dilution 1:100
Anti-mouse CD11a PE, (M17/4) Biolegend Cat# 101107; RRID:AB_312780 Validation https://www.biolegend.com/en-us/products/pe-anti-mouse-cd11a-antibody-355 Dilution 1:100
Anti-mouse CD11c APC, (N418) Biolegend Cat# 117310; RRID:AB_313779 Validation https://www.biolegend.com/en-us/products/apc-anti-mouse-cd11c-antibody-1813 Dilution 1:100
Anti-mouse SIRPα FITC, (P84) Biolegend Cat# 144006; RRID:AB_11204425 Validation https://www.biolegend.com/en-us/products/fitc-anti-mouse-cd172a-sirpalpha-antibody-7829 Dilution 1:100
Anti-mouse CD200R1 FITC, (OX-110) Biolegend Cat# 123909; RRID:AB_1227748 Validation https://www.biolegend.com/en-us/products/fitc-anti-mouse-cd200r-ox2r-antibody-5174 Dilution 1:100
Anti-mouse CD64 PE, (X54-5/7.1) Biolegend Cat# 139304; RRID:AB_10612740 Validation https://www.biolegend.com/en-us/products/pe-anti-mouse-cd64-fcgammari-antibody-6691 Dilution 1:100
Anti-mouse CD16/32 APC, (93) Biolegend Cat# 101326; RRID:AB_1953273 Validation https://www.biolegend.com/en-us/products/apc-anti-mouse-cd16-32-antibody-6282 Dilution 1:100
Anti-mouse F4/80 pacific blue, (BM8) Biolegend Cat# 123124; RRID:AB_893475 Validation https://www.biolegend.com/en-us/products/pacific-blue-anti-mouse-f4-80-antibody-4075 Dilution 1:100
Anti-mouse CD18 PE, (M18/2) Biolegend Cat# 101408; RRID:AB_312817 Validation https://www.biolegend.com/en-us/products/pe-anti-mouse-cd18-antibody-360 Dilution 1:100
Anti-mouse F4/80 APC, (BM8) Biolegend Cat# 123116; RRID:AB_893481 Validation https://www.biolegend.com/en-us/products/apc-anti-mouse-f4-80-antibody-4071 Dilution 1:100

Anti-mouse NK1.1 PE, (PK136) Biolegend Cat# 108708; RRID:AB_313395 Validation https://www.biolegend.com/en-us/products/pe-anti-mouse-nk-1-1-antibody-431 Dilution 1:100
Anti-mouse Ly6G FITC, (1A8) Biolegend Cat# 127606; RRID:AB_1236494 Validation https://www.biolegend.com/en-us/products/fitc-anti-mouse-ly-6g-antibody-4775 Dilution 1:100
Anti-rat IgG AF647, (Poly4054) Biolegend Cat# 405416; RRID:AB_2562967 Validation https://www.biolegend.com/en-us/products/alexa-fluor-647-goat-anti-rat-igg-minimal-x-reactivity-9252 Dilution 1:100
Anti-mouse F4/80 APC-Cy7 (BH8) Biolegend Cat#123118; RRID:AB_893477 Validation https://www.biolegend.com/en-us/products/apc-cyanine7-anti-mouse-f4-80-antibody-4072 Dilution 1:100
Anti-mouse Ly6G Alexa 647 (1A8) Biolegend Cat# 127610; RRID:AB_1134159 Validation https://www.biolegend.com/en-us/products/alexa-fluor-647-anti-mouse-ly-6g-antibody-4780 Dilution 1:100
Anti-mouse NK1.1 PE-Cy7 (PK136) Biolegend Cat# 108714; RRID:AB_389364 Validation https://www.biolegend.com/en-us/products/pe-cyanine7-anti-mouse-nk-1-1-antibody-2840 Dilution 1:100
Anti-mouse β-Actin, (AC-74) Sigma-Aldrich Cat# A2228-200UL; RRID:AB_476697 Validation https://www.sigmaaldrich.com/CA/en/product/sigma/a2228 Dilution 1:100
Anti-human IgG1,Fc specific AF647, (pAb) Jackson immune research Cat# 109-606-098 RRID:AB_2337899 Validation https://doi.org/10.1016/j.celrep.2021.110111 Dilution 1:100
Anti-mouse IgG AF647, (pAb) Jackson immune research Cat# 115-605-071 RRID:AB_2338909 Validation https://doi.org/10.1016/j.celrep.2021.110111 Dilution 1:100
Anti-human CD20, (S18015E) Biolegend Cat# 375502; RRID:AB_326565 Validation https://www.biolegend.com/en-us/products/purified-anti-human-cd20-antibody-19712 Dilution 1:100
Anti-mouse CD45 Alexa Fluor® 700 (30-F11) Biolegend Cat# 103128; RRID:AB_493715 Validation https://www.biolegend.com/en-us/products/alexa-fluor-700-anti-mouse-cd45-antibody-3407 Dilution 1:100
Anti-DYKDDDDK Tag APC, (L5) Biolegend Cat# 637308; RRID:AB_2561497 Validation https://www.biolegend.com/en-us/products/apc-anti-dykddddk-tag-antibody-8099 Dilution 1:100
Anti-Flag Tag, (M2) Sigma-Aldrich Cat# F1804-200UG; RRID:AB_262044 Validation https://www.sigmaaldrich.com/CA/en/product/sigma/f1804 Dilution 1:100
Anti-Myc Tag (9B11) Cell Signaling Technology Cat# 2276S; RRID:AB_331783 Validation https://www.cellsignal.com/products/primary-antibodies/myc-tag-9b11-mouse-mab/2276?__hsfp=725946328&__hssc=130705104.1.1613433600241&__hstc=130705104.9c49e44b73bd3bee6fa385653ecd7c96.1613433600238.1613433600239.1613433600240.1&Ns=product.currentLot.numberOfApplications%7C1&N=0+4294956287&Nrpp=30&fromPage=plp&_requestid=4942784 Dilution 1:100
Anti-mouse CD47 (Polyclonal) R and D Systems Cat# AF1866; RRID:AB_2074942 Validation https://www.rndsystems.com/products/mouse-rat-cd47-n-terminal-igv-like-extracellular-domain-antibody_af1866 Dilution 1:100
Anti-mouse CD47 (D3O7P) Cell Signaling Technology Cat# 63000; RRID:AB_2799637 Validation https://www.cellsignal.com/products/primary-antibodies/cd47-d3o7p-rabbit-mab/63000 Dilution 1:100
Anti-mouse CD319 (E5C4M) Cell Signaling Technology Cat# 98611; RRID:AB_2800306 Validation https://www.cellsignal.com/products/primary-antibodies/cracc-slamf7-cd319-e5c4m-rabbit-mab/98611 Dilution 1:100
mouse IgG2a isotype control (C1.18.4) BioXCell Cat# BE0085; RRID:AB_1107771
Anti-human CD25, (7G7) BioXCell Cat# BE0014 RRID:AB_1107617
Anti-mouse CD3 epsilon (145-2C11), Fc Silent Kappa Absolute Antibody Cat# Ab00105-6.4
Anti-mouse CD28 (D665), Fc Silent Kappa Absolute Antibody Cat# Ab00285-1.4
Recombinant anti-mouse SIRPa, (23) André Veillette, in-house, from hybridoma sequence
Recombinant anti-mouse SIRPa, (27) André Veillette, in-house, from hybridoma sequence
Recombinant anti-mouse SLAMF7, (4G2) André Veillette, in-house, from hybridoma sequence
Recombinant anti-human SLAMF7, (Z1) André Veillette, in-house, from hybridoma sequence
Recombinant anti-human SLAMF7, (Z8) André Veillette, in-house, from hybridoma sequence
Recombinant anti-human SLAMF7, (Z9) André Veillette, in-house, from hybridoma sequence
Recombinant anti-human SLAMF7, (Z10) André Veillette, in-house, from hybridoma sequence
Recombinant anti-human SLAMF7, (Z26) André Veillette, in-house, from hybridoma sequence
Recombinant anti-human SLAMF7, (Z27) André Veillette, in-house, from hybridoma sequence
Recombinant anti-human SLAMF7, (Z30) André Veillette, in-house, from hybridoma sequence
Recombinant anti-human SLAMF7, (Z46) André Veillette, in-house, from hybridoma sequence
Recombinant anti-human SLAMF7, (elotuzumab) André Veillette, in-house, from patent sequence
Recombinant anti-mouse SIRPa, (MY-1) André Veillette, in-house, from hybridoma sequence
Recombinant anti-mouse CD47, (MIAP301) André Veillette, in-house, from hybridoma sequence
Recombinant anti-human hSIRPa, (KWAR23) André Veillette, in-house, from patent sequence
Recombinant anti-human hSIRPa, (18D5) André Veillette, in-house, from patent sequence
Recombinant anti-human hSIRPa, (50A) André Veillette, in-house, from patent sequence
Recombinant anti-human hSIRPa, (40A) André Veillette, in-house, from patent sequence
Recombinant anti-human CD47, (B6H12) André Veillette, in-house, from patent sequence
Recombinant anti-human CD47, (AO-176) André Veillette, in-house, from patent sequence

Validation

The commercially available primary antibodies were validated by the vendors on their official websites. The antibodies generated in Dr. Veillette's lab have been validated by flow cytometry and western blot on wild-type vs specific knockout cells, and cells (293T, BI-141, EL-4) that over-expressed the specific proteins; by ELISA for the specific antigens. All the antibodies have been validated as cited in the manuscript.
Further details of antibody validation can be found at:
1, https://www.biolegend.com/reproducibility
2, https://www.thermofisher.com/ca/en/home/life-science/antibodies/invitrogen-antibody-validation.html
3, Patents (WO2017178653A2, US10851164B2, US20200095318, US7709610B2, EP2569013A2)
4, Chen, J. et al. SLAMF7 is critical for phagocytosis of haematopoietic tumour cells via Mac-1 integrin. Nature 544, 493-497 (2017).
5, Rhee, I., Davidson, D., Souza, C.M., Vacher, J. & Veillette, A. Macrophage fusion is controlled by the cytoplasmic protein tyrosine phosphatase PTP-PEST/PTPN12. Mol Cell Biol 33, 2458-2469 (2013).

Eukaryotic cell lines

Policy information about cell lines and Sex and Gender in Research

Cell line source(s)	L1210 (CCL-219), P815 (TIB-64), SP2/0 (CRL-1581), Raji (CCL-86), Daudi (CCL-213), MM.1S (CRL-2974), L929 (CCL-1), EL-4 (TIB-39), FO (CRL-1646), 293T (CRL-3216) and Phoenix-Eco (CRL-3214) were obtained from American Type Culture Collection.
Authentication	Cells were authenticated by the provider and verified in Dr. Veillette's lab by flow cytometry.
Mycoplasma contamination	The cell lines received were negative for Mycoplasma contamination and were immediately frozen upon initial receipt and expansion. Original frozen stocks were thawed regularly.
Commonly misidentified lines (See ICLAC register)	No commonly misidentified lines were used.

Palaeontology and Archaeology

Specimen provenance	Not applicable
Specimen deposition	Not applicable
Dating methods	Not applicable

☐ Tick this box to confirm that the raw and calibrated dates are available in the paper or in Supplementary Information.

Ethics oversight	Not applicable

Note that full information on the approval of the study protocol must also be provided in the manuscript.

Animals and other research organisms

Policy information about studies involving animals; ARRIVE guidelines recommended for reporting animal research, and Sex and Gender in Research

Laboratory animals	SIRPa KO, SFR KO, SLAMF7 KO, hSLAMF7 bacterial artificial chromosome transgenic, CD47 KO and RAG-1 KO mice were maintained in the C57BL/6J background. Sex and age-matched male or female mice between 8 and 12 weeks of age were used for experiments. Animals were housed in IRCM SPF (specific pathogen free) animal facilities and were fed with irradiated Global 18% Protein Rodent Diet, Inotiv, Madison, Wisconsin USA. Purified RO (reverse osmosis) water was provided ad libidum through an automatic water system (EDSTROM-Avidity Sciences , WI, USA). An Allentown PNC [Model PNC – positive/negative control, 160 cages (P/NC) individually ventilated cage system with Edstrom™ automated watering – Allentown Inc, Allentown, NJ, USA in ventilated racks and negative pressure] was used for housing, in a controlled microclimate environment at temperatures of 20-23°C with 40-60% humidity. An automated light system provided a light/dark cycle of 12h/12h. Animals were handled only in HEPA-filtered flow, type II class A Biosafety cabinets and in a 100% fresh filtered HEPA air ventilation room.
Wild animals	The study did not involve wild animals.
Reporting on sex	Both male and female were used in this study.
Field-collected samples	The study did not involve samples collected from the field.
Ethics oversight	Animal experimentation was approved by the Animal Care Committee of the Institut de recherches cliniques de Montréal and performed as defined by the Canadian Council of Animal Care.

Note that full information on the approval of the study protocol must also be provided in the manuscript.

Clinical data

Policy information about clinical studies

All manuscripts should comply with the ICMJE guidelines for publication of clinical research and a completed CONSORT checklist must be included with all submissions.

Clinical trial registration	Not applicable
Study protocol	Not applicable
Data collection	Not applicable
Outcomes	Not applicable

Dual use research of concern

Policy information about dual use research of concern

Hazards

Could the accidental, deliberate or reckless misuse of agents or technologies generated in the work, or the application of information presented in the manuscript, pose a threat to:

No	Yes	
☒	☐	Public health
☒	☐	National security
☒	☐	Crops and/or livestock
☒	☐	Ecosystems
☒	☐	Any other significant area

Experiments of concern

Does the work involve any of these experiments of concern:

No	Yes	
☒	☐	Demonstrate how to render a vaccine ineffective
☒	☐	Confer resistance to therapeutically useful antibiotics or antiviral agents
☒	☐	Enhance the virulence of a pathogen or render a nonpathogen virulent
☒	☐	Increase transmissibility of a pathogen
☒	☐	Alter the host range of a pathogen
☒	☐	Enable evasion of diagnostic/detection modalities
☒	☐	Enable the weaponization of a biological agent or toxin
☒	☐	Any other potentially harmful combination of experiments and agents

ChIP-seq

Data deposition

☐ Confirm that both raw and final processed data have been deposited in a public database such as GEO.

☐ Confirm that you have deposited or provided access to graph files (e.g. BED files) for the called peaks.

Data access links *May remain private before publication.*	Not applicable
Files in database submission	Not applicable
Genome browser session (e.g. UCSC)	Not applicable

Methodology

Replicates	Not applicable
Sequencing depth	Not applicable
Antibodies	Not applicable
Peak calling parameters	Not applicable
Data quality	Not applicable
Software	Not applicable

Flow Cytometry

Plots

Confirm that:

☒ The axis labels state the marker and fluorochrome used (e.g. CD4-FITC).

☒ The axis scales are clearly visible. Include numbers along axes only for bottom left plot of group (a 'group' is an analysis of identical markers).

☒ All plots are contour plots with outliers or pseudocolor plots.

☒ A numerical value for number of cells or percentage (with statistics) is provided.

Methodology

Sample preparation	Mouse macrophages, bone-marrow-derived macrophages (BMDMs) were generated by growing freshly isolated bone marrow cells for 7 days in medium supplemented with 30% (vol/vol) L929 cell-conditioned medium, as a source of colony-stimulating factor-1 (CSF-1). Human macrophages were produced from peripheral blood mononuclear cells, which were isolated from healthy donors using Ficoll-Paque PLUS (Cat# 36-101-6383, GE Healthcare), according to the manufacturer's protocol and as approved by the IRCM Human Ethics Board. Peripheral blood mononuclear cells were then seeded onto Petri dishes containing serum-free RPMI medium for 30 min. After gentle washes to remove non-adherent cells, adherent cells (which mostly represent monocytes) were differentiated into macrophages by culture in medium supplemented with 10% human serum and 10 ng ml-1 CSF-1 (Cat# 300-25, Peprotech) for 7 days. Mouse splenocytes were obtained by mashing mouse spleen against 70 micron celll strainer (Fisher 08-771-2). Mouse CD4+ or CD8+ T cells, depleted of natural killer T (NKT) cells using anti-NK1.1 monoclonal antibody (MAb), were purified from splenocytes by negative selection using the EasySep Purification Kits (Cat# 19852 or 19853, STEMCELL Technologies). Activated CD4+ T cells were obtained by stimulating CD4+ T cells with 4 micrograms ml-1 concanavalin A (Cat# C5275, Sigma-Aldrich) for 2 days, followed by expansion for 3 days in medium containing 50 units ml-1 interleukin-2 (Cat# 212-12, Peprotech). Activated CD8+ T cells were obtained by stimulating CD8+ T cells with 3 micrograms ml-1 Fc-silent anti-CD3 (145-2C11, Absolute Biotech Company) plus 1 micrograms ml-1 Fc-silent anti-CD28 (D665, Absolute Biotech Company) MAbs for 2 days.
Instrument	CyAn ADP analyzer and BD LSR Fortessa were used to collect flow cytometry data. BD FACSAria III was used for cell sorting.
Software	FlowJo v10.6.2 was used to analyze flow cytometry data.
Cell population abundance	When cells were sorted or enriched, the purity was confirmed by flow cytometry. The population purity is at least 95%.
Gating strategy	Flow cytometry analyses focused on detecting the expression level of different makers in cells. In all experiments, cells were first gated on single cells. Then, dead cells were excluded by gating on 7-AAD negative cells.

☐ Tick this box to confirm that a figure exemplifying the gating strategy is provided in the Supplementary Information.

Magnetic resonance imaging

Experimental design

Design type	Not applicable
Design specifications	Not applicable
Behavioral performance measures	Not applicable

Acquisition

Imaging type(s)	Not applicable
Field strength	Not applicable
Sequence & imaging parameters	Not applicable
Area of acquisition	Not applicable

Diffusion MRI ☐ Used ☒ Not used

Preprocessing

Preprocessing software	Not applicable

Normalization	Not applicable
Normalization template	Not applicable
Noise and artifact removal	Not applicable
Volume censoring	Not applicable

Statistical modeling & inference

Model type and settings	Not applicable
Effect(s) tested	Not applicable

Specify type of analysis: ☐ Whole brain ☐ ROI-based ☐ Both

Statistic type for inference (See Eklund et al. 2016)	Not applicable
Correction	Not applicable

Models & analysis

n/a	Involved in the study
☒	☐ Functional and/or effective connectivity
☒	☐ Graph analysis
☒	☐ Multivariate modeling or predictive analysis